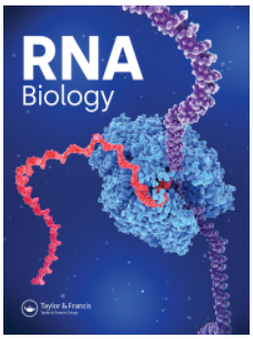

RNA Biology

ISSN: (Print) (Online) Journal homepage: www.tandfonline.com/journals/krnb20

Truncating the spliceosomal 'rope protein' Prp45 results in Htz1 dependent phenotypes

Kateřina Abrhámová, Martina Groušlová, Anna Valentová, Xinxin Hao, Beidong Liu, Martin Převorovský, Ondřej Gahura, František Půta, Per Sunnerhagen & Petr Folk

To cite this article: Kateřina Abrhámová, Martina Groušlová, Anna Valentová, Xinxin Hao, Beidong Liu, Martin Převorovský, Ondřej Gahura, František Půta, Per Sunnerhagen & Petr Folk (2024) Truncating the spliceosomal 'rope protein' Prp45 results in Htz1 dependent phenotypes, RNA Biology, 21:1, 1-17, DOI: 10.1080/15476286.2024.2348896

To link to this article: https://doi.org/10.1080/15476286.2024.2348896

RNA BIOLOGY
2024, VOL. 21, NO. 1, 1–17
https://doi.org/10.1080/15476286.2024.2348896

Taylor & Francis
Taylor & Francis Group

RESEARCH PAPER

OPEN ACCESS Check for updates

Truncating the spliceosomal 'rope protein' Prp45 results in Htz1 dependent phenotypes

Kateřina Abrhámová [a*], Martina Groušlová [a*], Anna Valentová [a], Xinxin Hao [b], Beidong Liu [b], Martin Převorovský [a], Ondřej Gahura [c], František Půta [a], Per Sunnerhagen [b], and Petr Folk [a]

[a]Department of Cell Biology, Faculty of Science, Charles University, Praha, Czech Republic; [b]Department of Chemistry and Molecular Biology, University of Gothenburg, Gothenburg, Sweden; [c]Institute of Parasitology, Biology Centre, Czech Academy of Sciences, České Budějovice, Czech Republic

ABSTRACT

Spliceosome assembly contributes an important but incompletely understood aspect of splicing regulation. Prp45 is a yeast splicing factor which runs as an extended fold through the spliceosome, and which may be important for bringing its components together. We performed a whole genome analysis of the genetic interaction network of the truncated allele of *PRP45* (*prp45*(1–169)) using synthetic genetic array technology and found chromatin remodellers and modifiers as an enriched category. In agreement with related studies, H2A.Z-encoding *HTZ1*, and the components of SWR1, INO80, and SAGA complexes represented prominent interactors, with *htz1* conferring the strongest growth defect. Because the truncation of Prp45 disproportionately affected low copy number transcripts of intron-containing genes, we prepared strains carrying intronless versions of *SRB2*, *VPS75*, or *HRB1*, the most affected cases with transcription-related function. Intron removal from *SRB2*, but not from the other genes, partly repaired some but not all the growth phenotypes identified in the genetic screen. The interaction of *prp45*(1–169) and *htz1*Δ was detectable even in cells with *SRB2* intron deleted (*srb2*Δi). The less truncated variant, *prp45*(1–330), had a synthetic growth defect with *htz1*Δ at 16°C, which also persisted in the *srb2*Δi background. Moreover, *htz1*Δ enhanced *prp45*(1–330) dependent pre-mRNA hyper-accumulation of both high and low efficiency splicers, genes *ECM33* and *COF1*, respectively. We conclude that while the expression defects of low expression intron-containing genes contribute to the genetic interactome of *prp45*(1–169), the genetic interactions between *prp45* and *htz1* alleles demonstrate the sensitivity of spliceosome assembly, delayed in *prp45*(1–169), to the chromatin environment.

ARTICLE HISTORY
Revised 13 December 2023
Accepted 24 April 2024

KEYWORDS
Synthetic genetic array analysis; spliceosome assembly; co-transcriptional splicing; chromatin modifiers; H2A.Z

Introduction

Splicing and transcription are interdependent

The processes of transcription and transcript maturation, including capping, splicing, cleavage, and polyadenylation are executed in immediate succession [1], which results in their interdependence and allows cells to regulate them coordinately [2–4]. Co-transcriptionality of splicing was established for both yeast and Metazoa [5–8], and various mechanisms were proposed to explain the coupling between splicing and transcription [1,5,9–11]. The biological significance of splicing resides in the complexity of the decisions *when* and *where* to splice. Accumulated evidence supports the view that these „decision algorithms" are embedded in part in the spliceosome assembly pathways [12], which are in turn dependent on the surrounding context [3,13,14]. This context depends on the interactions of chromatin domains, RNPs, nuclear proteins and small biomolecules, and represents a continuum with the gene expression system of the cell [15]. Indeed, co-transcriptional spliceosome assembly was shown to depend on chromatin modifiers, such as the histone acetyltransferase Gcn5 [16], the H2B ubiquitylase Bre1 [17], or the histone methyltransferase Set2 [18,19]. The component of the TBP binding module of the Gcn5/SAGA acetyltransferase complex, Spt8, interacted with the spliceosomal ATPase Prp5, which promoted pre-spliceosome formation. Through this interaction, Spt8 was able to affect the proofreading of suboptimal splicing substrates, mediating the interplay between transcription initiation, elongation, and splicing [20]. The methyltransferase Set2 recruited the adaptor Eaf3 through H3K36 methylation, which in turn enhanced the association of the spliceosomal Nineteen complex and Prp45, at least on some intron containing genes [19]. Transcription elongation factors, apart from regulating PolII kinetics, can also contribute to co-transcriptional spliceosome recruitment, as was shown for Spt5, part of the DSIF complex, which enhanced U5 snRNP association with intron containing genes [21].

CONTACT Petr Folk petr.folk@natur.cuni.cz Department of Cell Biology, Faculty of Science, Charles University, Praha 110 00, Czech Republic
*These two authors contributed equally to this work.
Supplemental data for this article can be accessed online at https://doi.org/10.1080/15476286.2024.2348896

Splicing factors have negative genetic interactions with alleles of chromatin regulators

Splicing factors and chromatin regulators display extensive genetic interactions, but the evidence for accompanying physical interactions is lagging (see Figure 2 in [1] and references therein; [18]). To account for the functional coupling between transcription and splicing, three mutually non-exclusive modes have been considered in the literature. The first mode was direct physical binding of splicing and transcription complexes. Some splicing factors were found to be in direct contact with chromatin components [13,24], regulating the distribution of chromatin modifications in Metazoa [25]. The second mode was colocalization through liquid-liquid phase separation, which could impact the local concentrations of components available for spliceosome assembly [26–28]. Finally, kinetic coupling was postulated to account for the findings that the speed of RNA PolII matched the speed of splicing [1,29,30]. In yeast, co-transcriptional splicing was reported to affect PolII progression [31], while transcription speed was shown to have an impact on splicing efficiency [10,29]. All three modes would be receptive to regulatory inputs, such as posttranslational modifications of the C-terminal domain of RNA PolII [32,33], changes of components which affect the properties of nuclear condensates [34–36], or chromatin modifications which impact RNA PolII elongation [37–39]. In addition to chromatin modifications, deposition and remodelling of histone variants, such as H2A.Z, were shown to be important for maintaining the heterochromatin/euchromatin boundaries [40] and proper gene activation [41–47].

Prp45/SKIP

Prp45/SKIP is a spliceosomal 'rope protein' spanning ~ 141 Å across the structure of the yeast/human spliceosome (Figure 1A; [51,53]). The protein contains regions of predicted intrinsic disorder and assumes an extended fold, contacting several splicing factors and all snRNAs involved in catalysis across the spliceosome [54,55]. Prp45 chain assumes similar conformation in all complexes where it is traceable, i.e. from B^{act} to post catalytic spliceosomes [54,56,57]. The protein's chain passes very close to the U2/U6 catalytic core, but mutations of this region in *S. cerevisiae* or *S. pombe* (SNWKN) had no apparent cellular phenotype ([58]; unpublished results). Parts of the protein were not resolved in EM models and may contact additional, not yet recognized partners.

Several structural elements stand out from the extended fold of Prp45. It is the loop-sheet motif in its N-region which wraps around Prp46, the motif which contacts the RES complex member Slt11/Ecm2, and a long helix which interfaces Cef1, Prp8, and Pml1 (RES). These motifs can be also predicted in AlphaFold (bypassing direct use of structural templates; [50]), suggesting that they form independently of other structures and may bind prospective partners. The extended regions between these motifs may act as 'linkers', contributing flexibility in the initial phases of spliceosome formation [59]. Prp45 may thereby increase the cooperativity of assembly of splicing components as well as promote phase separation.

The human homolog of Prp45, SNW1/SKIP, was implicated in extra-spliceosomal roles in transcription initiation (interacting with Ski, VDR, pRb [60,61] and elongation in Metazoa [62]). This effect can be rationalized by assuming that SKIP affects transcription through its interactions with the elongating RNA PolII holocomplex or through its participation in transcription related condensates. SKIP was found to interact with the elongation factor p-TEFb [62] and splicing factor U2AF65 [63], both of which bind elongating PolII [64,65]. The SNW1 homolog of *S. pombe* binds U2AF35 [66].

Our earlier data hinted at the 'rope' character of Prp45, when we found that the stepwise truncation of the essential splicing factor did not produce any discernible growth phenotype until the rather extensive ablation of 210 amino acids in *prp45*(1–169). Prp45(1–169) cells showed temperature-sensitive growth phenotype, cell wall deformities, and increased sensitivity to stressors [58]. At permissive temperature, pre-mRNAs of most intron containing genes in *prp45*(1–169) exceeded WT levels several fold [67], similarly to mutants of early spliceosome assembly step factors [68]. Using ChIP, we demonstrated that the extended chain of Prp45 is required for co-transcriptional spliceosome assembly, affecting U2 snRNP association with pre-mRNA and subsequent assembly steps. We considered the *prp45*(1–169) allele to be a tool with which to further probe the function of this splicing factor.

Here, we mapped the genetic interactions of the truncated allele *prp45*(1–169) genome wide. Some of the phenotypes were dependent on intron presence in the *SRB2*/*MED20* gene, which codes for the 'head' component of the Mediator complex [69]. Remarkably, the interaction with *htz1*Δ persisted in the *srb2*Δi background and was evident even with less truncated alleles of *prp45*. The results show the importance of *HTZ1* for coupling transcription and splicing and the regulatory significance of co-transcriptional splicing for low expression intron containing genes.

Materials and methods

Yeast strains, media, cultivation conditions

Yeast strains used in this study are listed in STab. S1. Cells were cultivated using standard cultivation conditions in YPAD (1% yeast extract, 2% peptone, 0.01% adenine, 2% glucose, and 2% agar for solid plates) or synthetic dropout medium (SD; Formedium) supplemented with appropriate amino acids, 2% glucose, antibiotics, and other drugs as needed. Mutations in *PRP45* were accomplished by homologous recombination of the integration cassette generated by PCR from the template plasmid pFA6a-3 HA-NatMX6 [70]. Intron deletion from *SRB2*, *HRB1* and *VPS75* was done using the '*delitto perfetto*' method [71]. In the first step, the intron sequence was replaced with the *URA3* gene and in the second step, the *URA3* gene was removed using synthetic oligonucleotides and 5-FOA selection. Successful intron removal was confirmed by PCR and sequencing. All oligonucleotides are listed in STab. S2. Strains carrying multiple mutations were

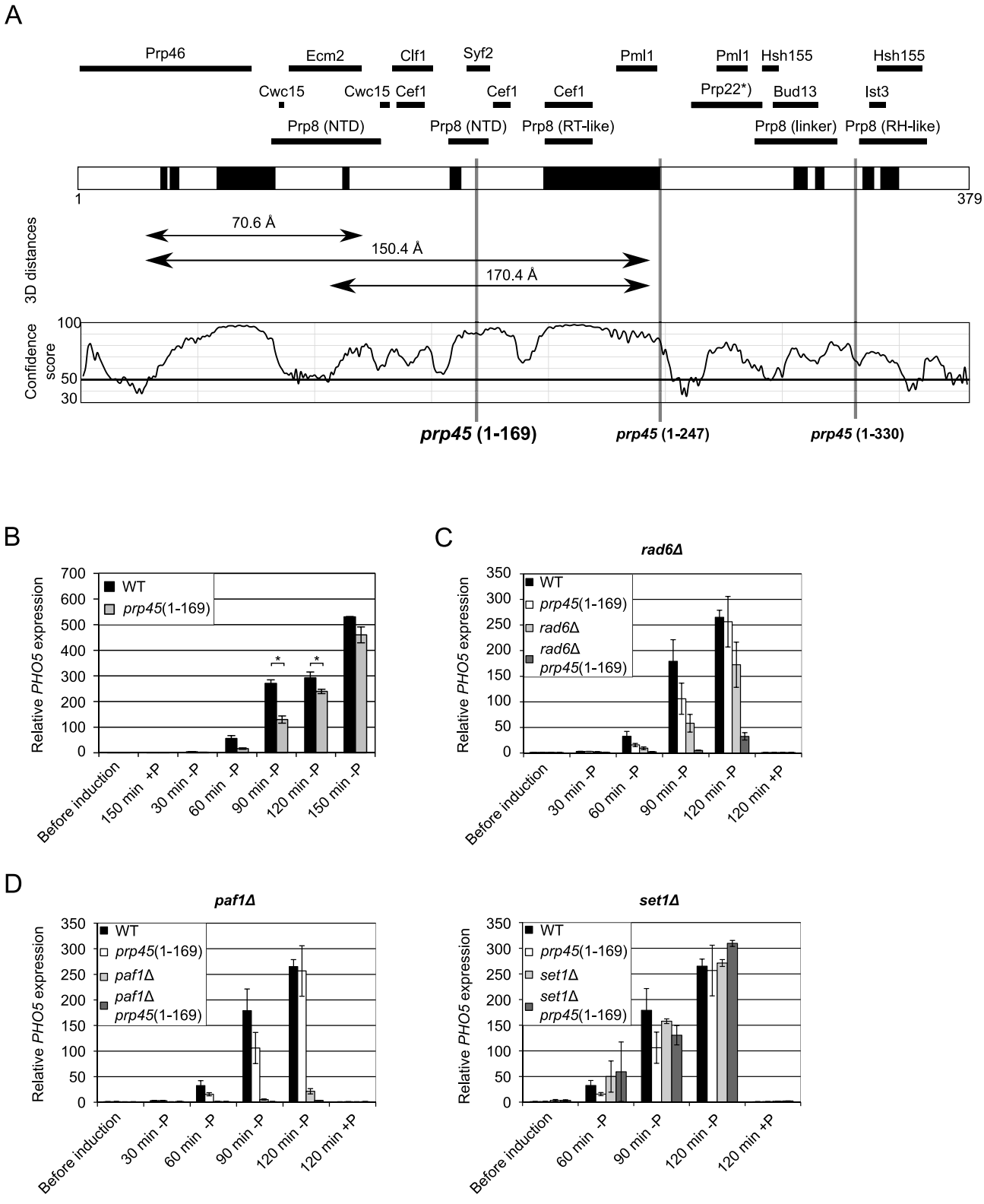

Figure 1. *prp45*(1–169) impaired the inducibility of *PHO5* synthetically with *rad6*. (A) primary structure and interacting partners of Prp45. Predicted helices are drawn as dark boxes over the primary structure. The 3D distances were taken from the spliceosomal P complex [48]. The diagram of disorder content is based on the values of the AlphaFold prediction [49]. Values below 50 were found to predict intrinsically disordered regions with high reliability [50]. The vertical lines over the primary structure indicate the extents of truncation of the variants used in this study. Interacting partners above the primary structure are drawn based on the proximity between Prp45 and the indicated components in the yeast spliceosomal structures [51]. Contacts with Prp46 (NTR) and Prp8 (tri-snRNP) are the most extensive. Contacts with Prp22 (marked with *), which are not resolved in the cryo-EM structures, are drawn according to the published two-hybrid data [52]. (B) induction of the *PHO5* gene in response to phosphate depletion was delayed in cells with truncated Prp45 as compared to WT. WT and *prp45*(1–169) cells were incubated in non-inducing conditions, washed, and transferred to a medium without phosphate. Total RNA was isolated at the indicated time points and reverse transcribed. RNA levels were quantified by qPCR, normalized to *TOM22* reference, and related to the signal obtained from WT cells before the shift. *p* values were calculated for the comparisons between WT and *prp45*(1–169) strains and a mutant strain using the t-test (see Methods). Stars indicate differences with $p < 0.05$. (C, D) the effect of *prp45*(1–169) on *PHO5* induction was tested with *rad6*Δ (C), *paf1*Δ, and *set1*Δ (D) using the same setup as in (B). Error bars represent standard deviations calculated from independent biological replicates. *p* values, which were obtained for comparisons between strains using the t-test with Holm correction for multiple testing, are listed in STab. 11 (see Methods).

prepared by de novo introduction of a specific mutation into the desired genetic background or by crossings as indicated in STab. S1.

To measure cell growth on the Bioscreen C (Oy Growth Curves Ab Ltd), pre-cultures were grown overnight at 30°C in an orbital shaker (5 ml) or a static incubator (honeycomb plate; 350µl). Cultivation was performed in 350ul of medium with high intensity shaking for 60 sec, alternated with pausing for 60 sec. O.D. at 600 nm was measured every 20 minutes. For VarioSkan Flash (Thermo Scientific) measurements, cells were incubated in 24 well plates in 700µl of medium inoculated with 5µl of overnight pre-cultures. The instrument settings were as follows: rotation speed 240 rpm, amplitude 17 mm, and O.D. at 600 nm. Measurements were taken every 10 minutes.

In phosphate shift experiments, cells were cultivated in synthetic medium to mid-log phase, washed three times with the same volume of prewarmed water, resuspended in phosphate free medium, and cultivated for the indicated times. Cells were then collected by centrifugation (1000 g for 3 min at RT) and frozen in liquid nitrogen. Samples were subjected to Northern blot or qPCR analyses (see below).

SGA analysis

SGA analysis was performed as described in [72] in two replicates. The query strain (KAY27) was prepared by introducing the mutation *prp45*(1–169) in the strain Y9072. Y8835 served as a control strain expressing the nourseothricin N-acetyl transferase cassette. The query and control strains were crossed with the deletion mutant array [73]. All manipulations were performed robotically using RoToR HDA (Singer Instruments) in 1536-dot format (four replicate spots per strain). The final plates were incubated at 30° and 35°C and the growth of the double mutant progeny was documented after one, two and three days of growth using a Canon PowerShot A640 camera. Colony sizes were analysed using computer scoring software (http://sgatools.ccbr.utoronto.ca/). Hits were confirmed by random spore analysis, measurements of growth rates in liquid culture, or by tetrad dissection after crossing the strains *de novo*. Except for hits where the colonies were consistently much smaller at all SGA plates across all temperatures, all other SGA hits were validated. Those that remained dubious were excluded or the double mutants were prepared de novo (see STab. S4 for details). Primary SGA data, list of hits containing their computed scores and verification status, and the results of the Gene Ontology (GO) term analysis are available in STab. S3, S4, and S5, respectively.

RNA analysis

RNA was isolated using the MasterPure Yeast RNA Purification Kit (Epicentre Biotechnologies), including the DNaseI treatment step, essentially according to the manufacturer's instructions. Reverse transcription was done using the RevertAid^{TM} First Strand cDNA Synthesis Kit (ThermoFisher) according to the manufacturer's protocol. Two µg of RNA were used as a template and reactions were primed with random hexamers.

qPCR was performed on a LightCycler 480 II (Roche). Each reaction consisted of 2 µl of HOT FIREPol® EvaGreen® qPCR Supermix (Solis Biodyne), 0.3 mM primers, and 1.5 µl of cDNA (total volume of 10 µl). Each sample was run in triplicates. Results were calculated using the $\Delta\Delta C_t$ method [74]. For statistical analysis, Student's t-test was employed using ΔCt data and the correction for multiple testing where appropriate (see STab. S11 for p-values). The calculations were performed with the 'R' statistical package version 3.2.3 (www.r-project.org/) using the t.test() function with parameters 'paired = FALSE, alternative = "two.sided"'. The function p.adjust() with Holm correction was used; $p < 0.05$ was considered significant.

Data analyses

RNA-seq data of the *prp45*(1–169) strain were published in [67] and are available from the Array Express Database (https://www.ebi.ac.uk/arrayexpress/) under accession number E-MTAB-5149. Where appropriate, RNA-seq data were normalized to obtain TPM (transcripts per million) values to account for transcript length and sequencing depth. TPM is described in http://www.arrayserver.com/wiki/index.php?title=TPM. Splicing efficiency was calculated as described in [75]. Briefly, splicing efficiency for each intron was determined using the formula: Efficiency = transread count/intron end base coverage (the 5'splice site was used in calculations). While the amount of transreads reflects mature mRNA abundance, intron coverage reflects pre-mRNA levels.

The yeast genetic interaction similarity network was generated by the spring-embedded network layout [4]. SAFE (Spatial Analysis of Functional Enrichment; [76]) was used to map the GO terms over the network of genetic interaction similarities. The select lists of genes were overlaid over the regions of genetic interaction similarity network using the web interface of TheCellMap database (https://thecellmap.org/).

Results

prp45(1–169) impaired the inducibility of the PHO5 and GAL1 genes

The *prp45*(1–169) truncation produced a mild phenotype, yet it frustrated the function of Prp45, so it could be used as a tool. In preliminary experiments, we found the *PHO* genes to be among the downregulated genes in the *prp45*(1–169) mutant. Because these genes were extensively studied with respect to gene induction and chromatin remodelling at promoters [77,78], we decided to examine their expression in more detail. We assessed the induction kinetics of several genes of the *PHO* regulon upon phosphate removal, which is known to induce the expression of factors regulating phosphate homoeostasis [77,78]. The tested genes exhibited an induction delay in the *prp45*(1–169) mutant. The shift, which was most pronounced in *PHO89*, *PHO12,* and *PHO5,* was also temperature dependent (Figure 1B and SFig. S1A).

Because of the capacity of SNW1/SKIP to affect both transcription initiation and elongation [60,62], we examined genetic interactions of *prp45*(1–169) with a panel of alleles of chromatin regulators which were known to interact with pre-mRNA splicing and processing. We found negative genetic interactions with a few alleles, including *bur2*Δ, *paf1*Δ, *lge1*Δ, and *rad6*Δ (SFig. S1B).

We next probed the inducibility of *PHO5* in some of the double mutants identified in our preliminary screen. The double mutant *rad6*Δ *prp45*(1–169) showed a synthetic effect (Figure 1C), while *set1*Δ, which did not synthetically impair the growth of *prp45*(1–169), did not impact *PHO5* inducibility (Figure 1D, right panel). *paf1*Δ, which interacted strongly with *prp45*(1–169) in the growth test, abrogated the induction to a great extent (Figure 1D, left panel; see also [79]). The inducibility defect of the *PHO5* gene was not limited to the *PHO* regulon. We found that the induction of the *GAL1* and *GAL10* genes upon the glucose to galactose nutrient shift was likewise hampered (SFig. S1C). We reasoned that the above induction defects were likely part of a general deficiency in gene inducibility, either in the general mechanism of transcription induction or in the permissibility of chromatin to the inducing effects of regulators.

We also noticed that *prp45*(1–169) had only limited impact on splicing of a reporter minigene derived from *ACT1* ([58]; SFig. S1D). The intron with WT splice sites showed no defect in the formation of spliced product, both in *prp45*(1–169) cells and in double mutants with *paf1* or *rad6*. Only the recombinant introns 3'gAG or 5'A3C, which were limiting for the first or second splicing step [80,81], respectively, showed splicing defects in the *prp45*(1–169) cells. The *rad6*Δ and *paf1*Δ mutants spliced the limiting substrates well and did not enhance the defect of *prp45*(1–169).

prp45(1–169) genetically interacted with alleles encoding chromatin regulators

We decided to take advantage of the thermosensitive allele *prp45*(1–169) (see Figure 1A) and examine its genetic interactions on the whole genome level. To this end, we employed the genome-wide SGA screen with a collection of 4291 viable deletion strains using *prp45*(1–169) as a query [72]. The deletion strains bearing *prp45*(1–169) were considered as hits when the average difference in colony size as compared to the control strain was at least 10% in at least one cultivation temperature. We found that *prp45*(1–169) negatively genetically interacted with 175 alleles of the deletion collection; a complete curated list of our SGA findings is available in STab. S4.

The genetic interactome was characterized by a high proportion of genes participating in transcription and chromatin regulation, and mRNA processing, which account for 33 and 14% of NGIs, respectively, as well as in vesicle trafficking, inositol and lipid metabolism, signalling, and DNA replication and repair (Figure 2A). A full list of NGIs according to GO terms is available in STab. S5. Several of the GO term categories showed high enrichment in NGIs, such as histone modifications and exchange, chromatin remodelling, regulation of RNA PolI transcription and nucleotide excision repair (SFig. S2A). As expected, the genes participating in spliceosome assembly, splicing and mRNA processing also showed high prevalence of NGIs. The NGIs included components of complexes regulating the chromatin environment – SWR1, INO80, SAGA, Paf1, Set3, Rpd3L/Rpd3S, and COMPASS. The genetic interaction of *prp45*(1–169) with *htz1*Δ was the strongest NGI that we found in our screen. The double mutant spores had problems germinating, but we eventually succeeded in isolating the strain, which was severely growth impaired (see Figure 2B upper left panel and Figure 4C). In addition to *htz1*Δ, SWR1C components (Figure 2B) and other chromatin regulators also showed strong double mutant phenotypes.

We compared our list of NGIs with previously published networks of genes involved in chromatin regulation and RNA metabolism. First, we analysed the distribution of *prp45*(1–169) NGIs among the clusters of chromatin regulators constructed in the perturbation analysis of Lenstra and co-authors [23]. Clusters containing members of the Paf1, Rad6/Bre1, Swr (including Htz1), and Set3 complexes showed the highest overlap with our NGI list (see Figure 1 in [23] and STab. S7). We constructed a matrix of all pairwise intersections of NGIs among the alleles from the enriched subclusters (37 alleles; STab. S7) and *prp45*(1–169) using the Multiple gene list comparator (STab. S8). The analysis showed that *prp45*(1–169) shared most genetic interactions with the Swr1 complex components *vps72*Δ, *swc3*Δ, *vps71*Δ, *arp6*Δ, and *swr1*Δ (sorted from the highest Jaccard index; [82]). The matrix is presented in Figure 2C as a heatmap, using the relative proportions of (identical NGIs)/(all NGIs) as a measure. The map illustrates that *prp45*(1–169) is an integral part of this highly interconnected group. The density of genetic interactions among the chromatin regulators and their genetic interaction partners in our map recapitulated the clusters based on transcriptomics profiles of deletion mutants (see the cladogram in Figure 1 in [23]). The connectivity among the SWR1 complex members plus *htz1*Δ (subclade 6D in STab. S7) and *prp45*(1–169) is further documented in a node diagram constructed in Cytoscape (SFig. 2B). Importantly, the impact of the gene deletions on *PRP45* expression was mostly minimal, with the lowest and highest mut/WT fold changes being 0.7 and 1.25, respectively (see Sheet2 in STab. S7), which included *htz1*Δ (0.8–0.86). In the *htz1*Δ dataset of Gu and co-authors [83], the mut/WT ratio for *PRP45* was 0.68.

Second, we examined the distribution of our NGIs among the splicing- versus retention-promoting gene deletions analysed by Sorenson and Stevens [84]. Using a unique single-cell yeast reporter, the authors tested 4,967 gene deletions for their effect on intron-bearing reporter cassettes. The gene deletions promoting intron retention included 17 NGIs, among which were the components of the Swr1 complex (*swc3*Δ, *arp6*Δ, *vps72*Δ, *vps71*Δ), *htz1*Δ, *spt8*Δ, and *set2*Δ (see Figure 7 in [84]; STab. S9). Mediator subunits Med9 and Med31 (*cse2*Δ and *soh1*Δ) were also part of this cluster. Only four null alleles promoted splicing, while 88% of *prp45*(1–169) NGIs were among the alleles which had only a mild effect on intron retention and remained outside of the clusters mentioned above.

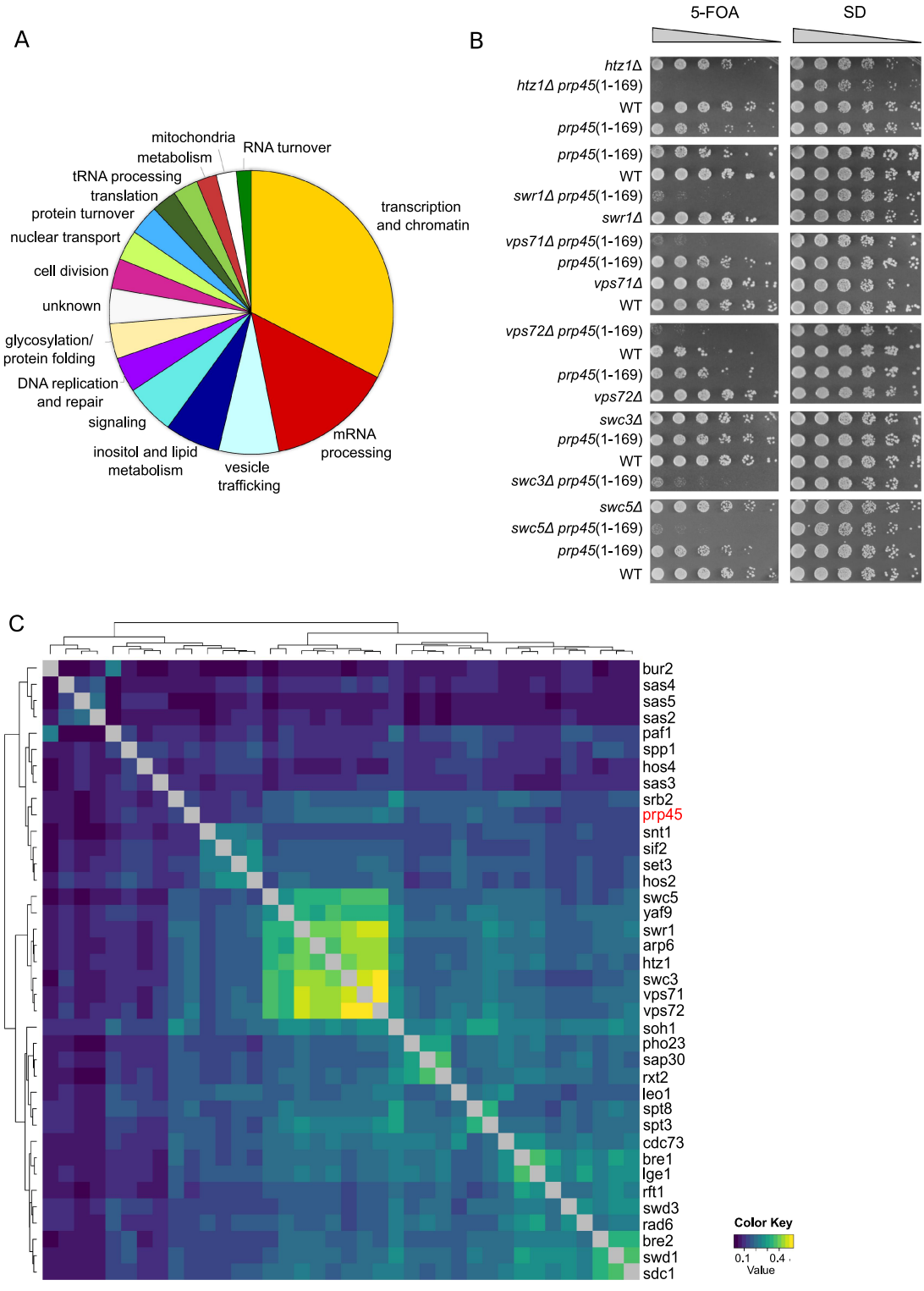

Figure 2. Synthetic genetic array analysis revealed strong negative genetic interactions of *prp45*(1–169) with genes involved in transcription and chromatin regulations. (A) pie-chart of manually curated categories illustrating the proportions of negative genetic interactions (NGIs) of *prp45*(1–169). The categories 'transcription and chromatin' and 'RNA processing' represent 33% and 14% of the NGIs found. Genes were grouped into categories using their GO terms as listed in STab. 6. (B) the *prp45*(1–169) allele had strong negative interactions with deletions of *HTZ1* and *SWR1* complex members. *prp45*(1–169) mutant cells were crossed with *htz1*Δ, *swr1*Δ, *vps71*Δ, *vps72*Δ, *swc3*Δ, and *swc5*Δ strains from the yeast deletion collection. Haploids with indicated combinations of mutations obtained from tetrad dissections of diploid strains harbouring an *URA3* plasmid with full length *PRP45* (p416ADH-His6-PRP45; [22]) were cultivated to the mid-log phase, serially 5× diluted and spotted on SD plates and SD plates with 5-FOA to get rid of the complementing plasmid. (C) *prp45*(1–169) shares a high proportion of its genetic interactions with other components of transcription and chromatin regulatory complexes. We overlaid the NGIs of *prp45*(1–169) onto the network of 165 chromatin regulators constructed in a previously published perturbation analysis [23]. The parts of the network which were enriched for the NGIs of *prp45*(1–169) (see STab. 7) were re-clustered, using the relative proportions of shared NGIs/all NGIs as a measure (increasing Jaccard indexes were used to cluster the heat-map). As a data source of NGIs genomewide, BioGRID (*S. cerevisiae*; thebiogrid.Org; downloaded 210127) categories 'negative genetic', 'synthetic growth defect', 'synthetic lethality' and 'phenotypic enhancement' were used. Multiple gene list comparator tool (https://www.molbiotools.com/listcompare.Php) was employed for the comparisons between genetically interacting genes and the calculation of Jaccard indexes. Interaction profiles of individual genes were hierarchically clustered and visualized as a heatmap.

Last, we compared the overlap of our NGI list with mRNA surveillance genes, which were functionally analysed by Sun and co-workers [85]. These authors used metabolic RNA labelling to cluster 46 surveillance factors according to their effects on mRNA degradation rates. Most NGIs of *prp45* (1–169) overlapped with a cluster containing components of the LSM1–7 complex (*lsm1*Δ, *lsm6*Δ, *lsm7*Δ), which targets RNA substrates for decapping, *pat1*Δ, an enhancer of decapping, and *pop2*Δ, a deadenylation factor (see Figure 5 in [85] and the complete list of overlaps in STab. S10). In contrast, we did not find GIs with components of cytosolic NMD pathway *xrn1*Δ or *upf3*Δ (SFig. S3A) and these NMD alleles did not produce any synthetic effect with respect to pre-mRNA accumulation when tested as double mutants with *prp45*(1–169) on *ECM33* [88].

prp45(1–169) preferentially impacted mRNA levels of low expression intronic genes

The truncation *prp45*(1–169) had only a modest effect on the transcriptome as a whole as judged from mean total RNA counts compared between mutant and WT [67]. We found 285 differentially expressed genes, out of which 17 were DOWN > 2 times and 9 were UP > 2 times. The lowest and highest log2(fold change) values were −2.7 and + 2.9. Among the differentially expressed genes, 33 contained an intron and 12 of these were ribosomal protein genes. Using our workflow for the calculation of splicing efficiency [75,89], we re-examined the *prp45*(1–169)-affected transcripts in comparison with our SGA hits and other features of intron containing genes in the literature (Figure 3). The pipeline was used to identify potential splice sites genome wide and calculate splicing efficiency as ratios of transread count/intron first base coverage. To characterize the effect of the truncation on mRNA levels, differentially scored transread ratios mut/WT were evaluated (see Methods). For most intron containing genes, these ratios were buffered around WT levels (1.1–0.8). We noticed, however, that the transread ratios decreased more substantially in intron containing genes with low levels of expression. The downregulated differentially scored transreads are referred to as 'subset_45' in the text (Figure 3A). Unlike the transread ratios, the relative splicing efficiencies in the mutant were uncorrelated with gene expression levels (Figure 3B). Considering intron length, subset_45 genes clustered with short intron-containing genes (Figure 3C), and the graph recapitulated the pattern from Figure 3A. This is probably because most intron containing RPGs, which are highly expressed, have longer introns (>200 nt), whereas non-RPGs cluster at short intron lengths.

To compare the subset_45 genes with our SGA hits, we used the NGI profile similarity map of *Saccharomyces cerevisiae* (Figure 3D [4,90–92]. Genetic interactions between categories of chromatin regulators and components of gene expression/surveillance systems were analysed using Cytoscape [93]. We compared the projections of our SGA hits, the subset_45 genes, and the complete set of intron containing genes. Clearly, only the SGA hit map overlapped the clusters of genes which are associated with mRNA processing, chromatin, and transcription (Figure 3D).

To identify features which would characterize the subset_45 genes, we looked into published data on co-transcriptional splicing efficiency [5], Htz1 levels measured by ChIP [83], or relative nucleosome turnover rates [87]. The graphs in Figure 3E, F show the distribution of the differentially scored transreads (see above; genes in red) in the datasets. Relative mRNA versus co-transcriptional splicing efficiency plot (= parameter 'observed delta' calculated in [5]; Figure 3E) showed that the genes with the highest parameter values (= highly efficiently spliced co-transcriptionally; observed delta between 0.7 and 1) are the least affected in the *prp45*(1–169) mutant. These genes are enriched in RPGs and thus highly expressed (out of 54 genes with 'observed delta' value > 0.8, 38 are RPGs).

Next, we compared our RNA-seq data with the data on Htz1 levels measured by Gu and co-workers ([83]; Figure 3F). In the *prp45*(1–169) mutant, genes containing very low Htz1 signal at transcription start site clustered at higher average relative mRNA than the rest of intron containing genes. This clustering again reflects the properties of RPGs – most of the genes with Htz1 ChIP signal below '8' are RPGs. When the intron containing genes were sorted according to expression level, the highest expressors showed the lowest Htz1 ChIP-Seq signal around transcription start site and the lowest antisense transcription (see SFig. 3B).

Finally, the scatter plot of relative mRNA versus relative nucleosome turnover at transcription start sites (Z-scores; [87]) showed that our differentially scored transreads tend to be enriched among high turnover rate genes (genes with low Z-scores; Figure 3G). As Dion and co-workers demonstrated, high nucleosome turnover correlated with increased Htz1 content. We found no dependence of relative splicing efficiency on Htz1 content, co-transcriptional splicing efficiency, or the length of intron or ORF (SFig. 3C).

Intron deletion of SRB2 repaired part of the phenotypes of prp45(1–169) and double allele mutants

prp45(1–169) reduced mRNA levels of a group of low expression intron containing genes, which could have contributed to the synthetic interactions that we observed. We tested this hypothesis by deleting introns of three such genes and measuring the phenotypes of the intronless mutants. We prepared intronless knockins (Δi) of genes coding for Hrb1, poly(A+) RNA-binding protein involved in spliced mRNA export; Vps75, histone binding HAT activator participating in DSB repair; and Srb2, subunit 20 of the Mediator complex [69], all of which have functions related to RNA metabolism. Intron deletions of either of these genes increased their mRNA levels in the *prp45*(1–169) background, with *SRB2* reaching ~ 2-fold excess over WT mRNA (SFig. S4A-I). Neither of the knockins influenced the growth of *prp45*(1–169) mutants (SFig. S4A-II and Figure 4B).

We then examined the effects of intron deletions on double and triple mutants, re-testing some of the alleles that we found previously in the SGA screen. Intron deletions of either *HRB1* or *VPS75* showed negligible impact on the growth phenotypes of *rad6*Δ, *paf1*Δ, or *gcn5*Δ as single or *prp45*(1–169) double mutants. By contrast, *srb2*Δi partially rescued the growth defect in *prp45*(1–

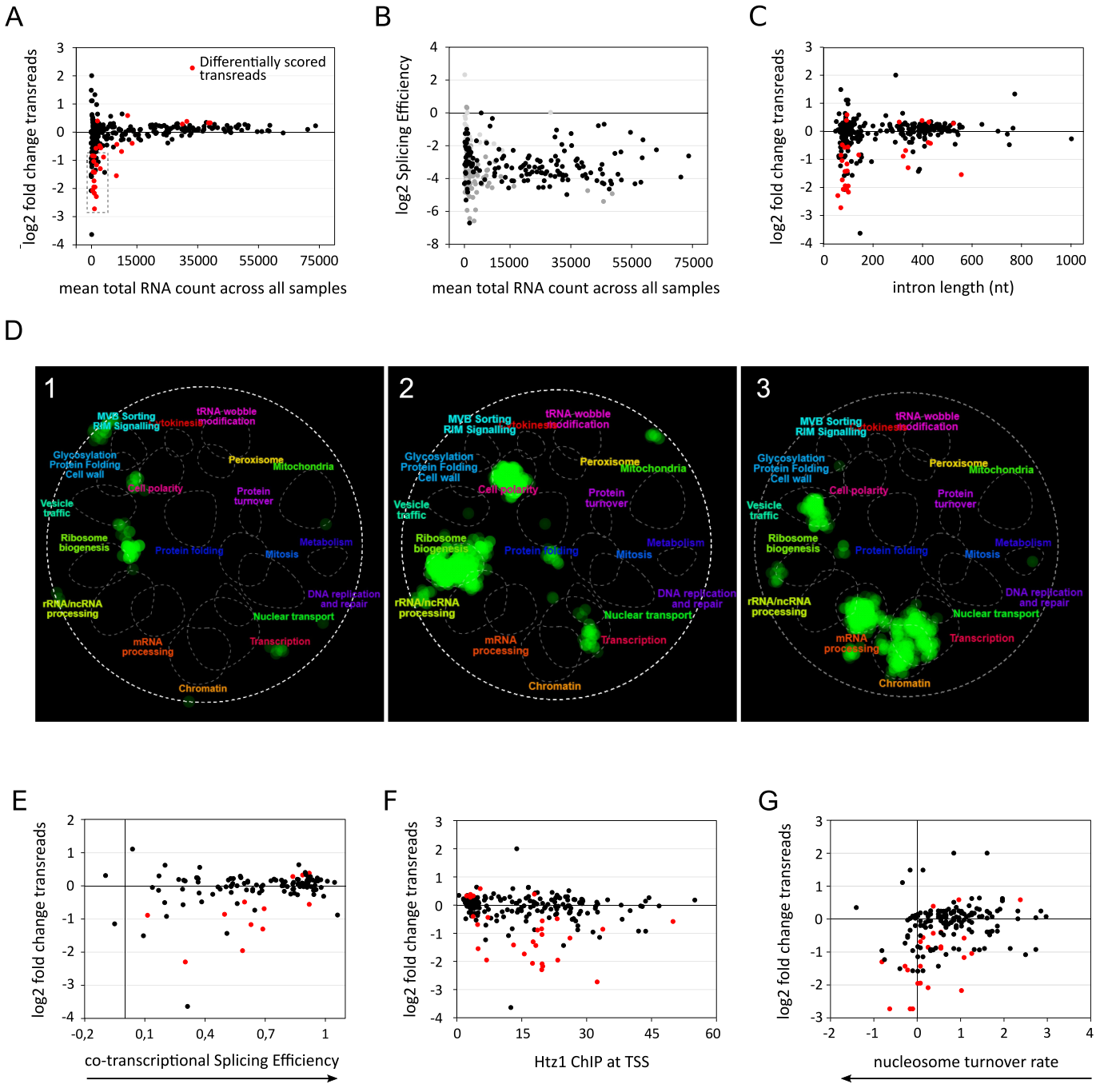

Figure 3. Negative genetic interactions of *prp45*(1–169) do not overlap with genes impacted on mRNA levels. To compare the genetic interactions of *prp45*(1–169) with the effect of the *prp45*(1–169) mutant allele on transcription, we plotted mRNA levels of intron containing genes as transread ratios mutant/WT, or splicing efficiency, using previously published RNA-seq data and our workflow [67,75]. (A) scatter plot shows the effects of *prp45*(1–169) on mRNA levels of intron containing genes, expressed as transread ratios mutant/WT, plotted against mean gene expression levels (total RNA count across all samples). Differentially scored transreads are shown in red. (B) for comparison, the effects of *prp45*(1–169) on splicing efficiency (S.E.) is plotted as in (A). Splicing efficiency was calculated by dividing transread counts by 5′ intron end first base coverage and expressed as mutant/WT ratios. Black data points are genes with sufficient coverage in both WT and mutant strain, i.e. ≥5 transreads and ≥5 reads covering intron end base. Gray data points represent genes which did not fully meet our criteria of sequence read data coverage (see S Fig.3A for details). (C) scatter plot showing relative transread ratios of intron containing genes (same data set as in (A)) as a function of intron length. (D) Genetic interaction enrichment landscapes generated using SAFE annotated genetic interaction similarity network of *S. cerevisiae* [4,76]. The maps were obtained from the web interface of TheCellMap database (https://thecellmap.org/). Downregulated differentially scored transreads of *prp45*(1–169) (Subset_45_genes) (STab. 12) (1), complete set of intron containing genes of *S. cerevisiae* (STab. 13) (2), and all NGIs we found (SGA hit list including manually curated alleles; STab. 14) (3) were visualized in green overlay using the interface. NGIs of *prp45*(1–169) but not the subset_45 genes showed overlap with the subnetworks of transcription and chromatin regulators. (E)–(G) relative mRNA levels of intron containing genes (same data set as in (A)) were plotted as a function of splicing and chromatin related parameters measured previously. Relative co-transcriptional efficiency (taken from [5]) (E), relative Htz1 density at transcription start sites (TSS) of genes [83] (F), and relative nucleosome turnover at transcription start sites [87] (G) were plotted on the x axis. Only the genes present in both datasets used for the comparison are shown. In (F), the graph does not show the gene YJR145C (coordinates 9.06112; 0.017245623). The parameter 'observed delta' increases with increasing co-transcriptional splicing efficiency ('1' = 100% co-transcriptional splicing). The parameter 'Z-score' increases with decreasing nucleosome turnover. Highly expressed genes, which are mostly ribosomal protein coding genes, cluster at longer intron length (in C), high co-transcriptional splicing efficiency (in E), low levels of Htz1 at transcription start sites (in F), and low relative nucleosome turnover at transcription start sites (in G). See text for discussion.

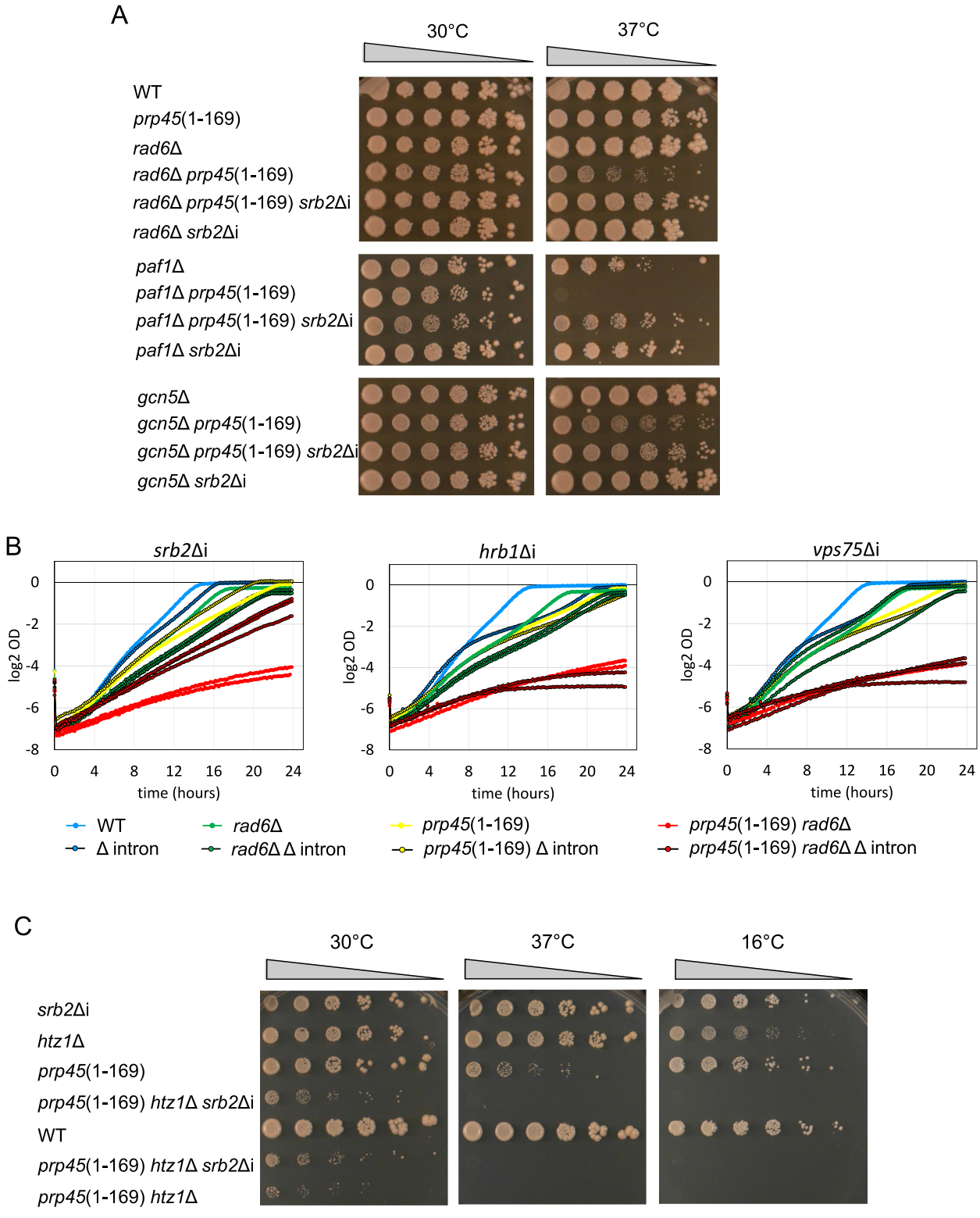

Figure 4. Intron deletion of *SRB2* repaired part of the growth defect of *prp45*(1–169). (A) intron deletion in *SRB2* partially repaired the growth defects of *prp45*(1–169) double mutants carrying deletions of *RAD6*, *PAF1*, and *GCN5*. Cells were cultivated to mid-log phase, serially diluted (ratio 1:4), spotted onto YPAD plates, and incubated at 30°C or 37°C for 6 days. (B) intron deletion in *SRB2*, but not in *HRB1* or *VPS75*, partially repaired the growth phenotype of *prp45*(1–169) *rad6*Δ double mutant. The growth of liquid culture in the YPD medium at 37°C was measured in VarioSkan. (C) *SRB2* intron removal had only negligible capacity to rescue the strong negative genetic interaction between *htz1*Δ *and prp45(1–169)*. Cells were cultivated to mid-log phase, serially diluted (ratio 1:4), spotted onto SD plates containing 5-FOA to dispose of complementing plasmid (p416ADH-His6-PRP45; [22]), and incubated at 30°C, 37°C, or 16°C for 7 days.

169)*rad6*Δ and *prp45*(1–169) *gcn5*Δ at 37°C, while it almost fully repaired the growth defect of *prp45*(1–169) *paf1*Δ (Figure 4A, B). Intriguingly, *srb2*Δ negatively genetically interacts with *gcn5*Δ but not with either *rad6*Δ or *paf1*Δ (BioGRID Version 4.4.223). The genetic interaction between *prp45*(1–169) and *htz1*Δ was strong even in the *srb2*Δi background, despite partial growth improvement of *prp45*(1–169) *htz1*Δ *srb2*Δi at 30°C (Figure 4C). We did not observe any growth of the triple mutant at 37°C or 16°C.

We also tested the effect of intron deletions on the induction delay of *PHO5* (Figure 1) and found that intron deletion of *SRB2*, but not *HRB1* or *VPS75*, repaired the kinetic defect caused by *PRP45* truncation (SFig. 4B). Decreased Srb2 was thus most likely the cause of the delayed induction seen with *PHO* and *GAL* genes (see Figure 1B and SFig. 1B), as they depend on Mediator recruitment to achieve full activation [94–96].

Less extensive truncation of Prp45 still exhibited a synthetic phenotype with htz1

Because of the strong synthetic growth defect of *prp45*(1–169) *htz1* mutant (Figure 4C), we constructed less extensive *PRP45* truncations (see truncation extents in Figures 1A&5A) and compared their phenotypes with the *prp45*(1–169) version. Single alleles *prp45*(1–247) and *prp45*(1–330) had no apparent growth defects at 16/30/37°C (Figure 5B), but they still accumulated excess levels of pre-mRNAs. The extent of pre-mRNA accumulation depended on Prp45 truncation but was not proportional to its extent, i.e. it was more severe in *prp45*(1–330) than in *prp45*(1–247) (Figure 5D). This would suggest that the truncation between aa 247 and 330 impaired the recruitment of some factors which inhibited retention. Alternatively, the Prp45 chain between aa 247 and 330 could interfere with the spliceosome assembly process due to the lack of the protein's C-terminus.

Allele *prp45*(1–330) showed genetic interaction with *htz1*Δ on the level of growth at 16°C. This phenotype was not repaired by *SRB2* intron deletion (Figure 5C). Importantly, *prp45*(1–330) also showed synthetic effect with *htz1*Δ on the level of pre-mRNA accumulation. We measured pre-mRNA and mRNA levels of *ECM33*, which is an efficiently spliced gene, and *COF1*, which is spliced less efficiently, and found the effects in both genes. Even the least extended truncation of *PRP45* thus resulted in genetic interaction with *htz1*Δ on the level of pre-mRNA accumulation (Figure 5E).

The hyperaccumulation of pre-mRNA, brought about by truncated *prp45* alleles, depends on the degree of truncation. Intriguingly, the defect can be repaired in part by lowering the demand for spliceosomes. We showed this by incubating cells with the TOR1C inhibitor rapamycin, which inhibits the transcription of RPGs in yeast via a feedback mechanism [97,98] (SFig. 5). Stalling of RPG transcription and splicing then lowers the demand for spliceosomes, as splicing of RPGs represents most of the splicing in *S. cerevisiae*. Rapamycin treatment lowered the high pre-mRNA levels of *ECM33* and *ACT1* in the mutants, but the pre-mRNAs remained at > 2 times WT levels, even after 30 minutes of incubation. This suggests that there are at least two components of the defect, one of which is rescued by increasing the availability of the spliceosomal components.

Discussion

Genetic interactions of prp45(1–169) overlap with the networks of chromatin regulators

Because of its flexibility and propensity to interact with multiple partners, Prp45 could bring together components during spliceosome assembly as well as couple splicing to other processes [19,51,53,99]. The truncation *prp45*(1–169), which drastically lowered the valency of this linker protein (see Figure 1A), was nevertheless viable in *S. cerevisiae* and produced only a mild phenotype (see Introduction; [58,67]). Notably, C-terminal truncations of Prp45 became lethal when the N-terminus was also ablated [58]. In this study, we performed an SGA screen to identify negative genetic interactions of a truncated version of *PRP45* (*prp45* (1–169)). Our data extend the networks of genetic interactions between splicing and transcription related factors, chromatin remodellers and modifiers observed previously [1,46,47].

The *prp45*(1–169) genetic interaction map that we obtained revealed *htz1*Δ and SWR1 complex components as the strongest interacting alleles (Figure 2). The histone variant Htz1 of *S. cerevisiae* (H2A.F/Z family of H2A variants) is deposited mostly in -1 and +1 nucleosomes at RNA PolII promoters, and its controlled turnover is important for proper gene activation [41,42,100,101]. Chromatin remodelling complexes SWR1C and INO80C are responsible for its deposition and targeted eviction, respectively. Alleles of SWR1C components and *htz1*Δ were reported to interact genetically with other splicing factors in *S. pombe* and *S. cerevisiae* [4,46,47]. A genetic screen with *swr1* in *S. pombe* identified splicing complexes across the splicing cycle, as well as *htz1* (*pht1* in *S. pombe*), Mediator complex and pTEFb, as enriched for NGIs [46]. In *S. cerevisiae*, targeted genetic screen with *htz1* found NGIs with alleles from all major splicing subcomplexes. Deletions of U2 snRNP related *MSL1*, *LEA1*, or *SNU17* conferred synthetic lethality [47]. The effect of *htz1* deletion on splicing efficiency was measured [47], but it was much less severe than the phenotype of *prp45*(1–169). We did not find any correspondence between the two data sets.

There is a notable discrepancy between the ample genetic interactions connecting the alleles in splicing and chromatin GO_TERM categories and the relatively fewer instances of documented physical coupling between proteins (see Figure 2 in [1] and references therein). Nevertheless, overlaps in genetic networks are interpreted in the literature to reflect functional similarities [90]. For example, general transcription factors show gene specific defects upon deletion, which can be used to cluster them to reveal functional interconnections [102,103]. We noticed that the alleles of chromatin regulators that negatively genetically interacted with *prp45*(1–169) form a highly connected group ([23]; see Figure 2D). Remarkably, the extent of connectivity of *prp45*(1–169) to nodes of the mentioned subnetwork is similar to the number of edges among the chromatin components themselves, suggesting functional involvement of Prp45 (see both the subcluster 6D diagram in SFigure 2C as well as our reclustered heatmap in Figure 2C).

Besides the SWR1 and INO80 complexes, several other heterooligomers of chromatin regulators were enriched in NGIs with *prp45*(1–169), such as the complexes of Paf1 [104,105], Rad6/Bre1 [106], Set1/COMPASS [107,108], Set3/Rpd3L [109], and Set2-Rpd3S [18,110]. All of these complexes are known to couple transcription with transcript processing through the changes of chromatin environment [111,112] and

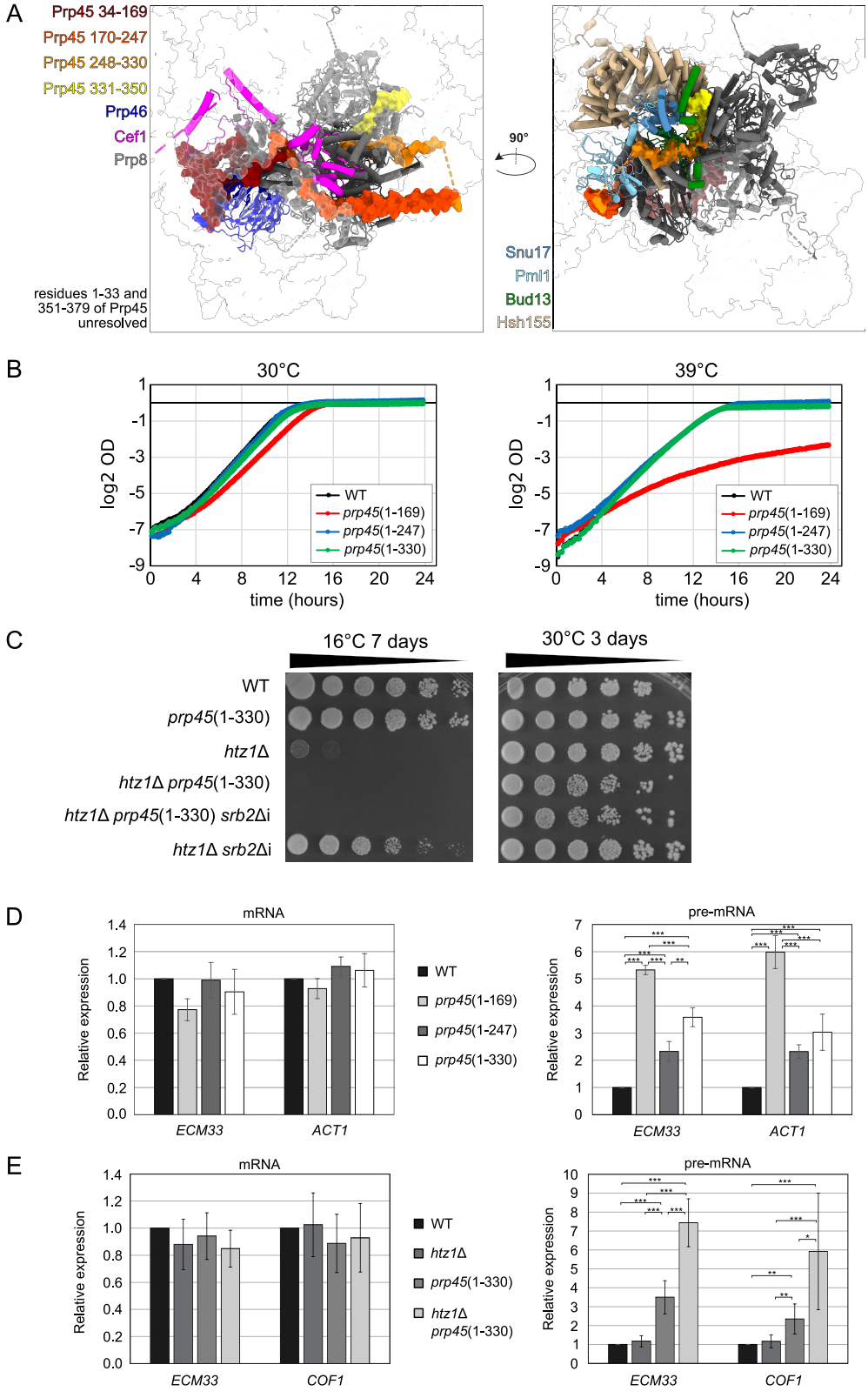

Figure 5. Less extensive truncation of Prp45 is sufficient to cause *htz1*-dependent pre-mRNA accumulation. (A) extended chain of Prp45 connects distinct parts of the spliceosomal architecture. In yeast B^{act} spliceosome (structure 5gm6; [54]), Prp45 contacts extensively Prp8 (grey) and more than 10 other proteins. We highlighted Prp46 (dark blue), Cef1 (purple), Bud13 (green), Snu17 (blue grey), Pml1 (light blue), and Hsh155 (ocre). The Prp45 fragments are coloured in dark red (1–169), orange (170–247), light orange (248–330), and yellow (331–350). The complex was visualized using ChimeraX [86]. Prp45(1–169) lacks parts of the chain that lines the interface between Prp8 (RT-like domain) and Cef1 (left). Prp45(1–247) is devoid of the contacts to the RES complex components (Pml1, Snu17 and Bud13) and the RNAse H-like domain of Prp8 (right). Truncation of the C-terminal 49 amino acids in Prp45(1–330) should impinge on the interactions with Prp8, Ist3, and Hsh155. Amino acids 1–30 and 350–379 (C-term) were not resolved in the structure and may contain additional interacting partners. (B) growth rate comparison of *prp45*(1–169), *prp45*(1–247), and *prp45*(1–330) cells. Cultivations in YPAD at 30°C were monitored using VarioSkan. In contrast to *prp45*(1–169) cells, the growth of *prp45*(1–247) and *prp45*(1–330) mutants was indistinguishable from the WT strain. (C) Intron deletion of *SRB2* partially repaired the cold sensitive growth phenotype of *htz1*Δ mutant but not of the double mutant *htz1*Δ *prp45*(1–330). Cells were cultivated to mid-log phase, serially diluted (ratio 1:4), spotted onto YPAD plates, and incubated

a number of their components genetically interact with *htz1*Δ. *rad6*Δ or *bre1*Δ is lethal in the absence of *HTZ1* [113], which hints at partial redundancy of H2B ubiquitylation and H2A.Z deposition. *set3*Δ also becomes growth limiting in *htz1* knockout, with loss-of-function suppressors being the SWR1 complex, the H2B deubiquitination module of SAGA, and Set1, among others [109].

Expression of low copy-number genes is particularly sensitive to prp45(1–169) truncation

Prp45 truncation resulted in the decrease of splicing efficiency for most intron containing genes, while the span of the splicing efficiency levels remained like WT. While splicing efficiency seems to have been affected globally, more pronounced decreases of mRNA levels were mostly confined to low expression genes (subset_45; Figure 3A). Two non-exclusive possibilities can be considered. The mutation could have a gene specific effect, similar to what was found for general splicing factors in *S. cerevisiae* [114]. However, we did not find any correlations which would hint at any common intronic feature of the affected genes in the subset_45. Alternatively or in part, Prp45 truncation could impair splicing (spliceosome assembly) globally, leading to generalized splicing efficiency decrease. The low expression genes would then be disproportionately affected because of their lower capacity to adjust turnover rates and thus buffer mRNA levels (see Fig 7 in [115]).

Splicing of the Mediator component may explain part of the prp45(1–169) phenotype

Intron deletion of the Mediator component *SRB2* repaired part of the growth phenotype of *prp45*(1–169)-interacting alleles (Figure 4). It should be noted that *srb2*Δi elevated *SRB2* mRNA levels to ~ 2 times WT levels, so some of the effects might be caused by the overexpression (SFig. S4A-I). While Srb2 decrease (=defect in Mediator function) may explain part of the negative synthetic growth defects of the SGA-positives, the *srb2*Δi does not repair the phenotype fully and is therefore unlikely to explain the whole NGI set. Also, the NGIs of the two alleles do not overlap. Notably, *SRB2* intron removal partly repaired the cold sensitivity of *htz1*Δ, but not of the *htz1*Δ *prp45*(1–330) double mutant (Figure 5C). *SRB2* mRNA levels in *htz1*Δ were previously found to be similar to WT [47], but because *SRB2* intron is spliced inefficiently, its deletion may lead to *SRB2* mRNA increase in *htz1*Δ. Similarly to *prp45*(1–169) *htz1*Δ *srb2*Δi, the *prp45*(1–330) *htz1*Δ *srb2*Δi mutant showed synthetic growth defect at 16°C, which was independent of *SRB2* splicing. The genetic interaction between *htz1*Δ and *prp45* can thus be demonstrated under conditions where just the C-terminal 49aa of Prp45 are ablated and it persists in the *srb2*Δi background.

SRB2 splicing was reported to be highly dependent on the functioning of the RES complex [116]. This is intriguing as Prp45 contacts the RES components in the spliceosome (Figure 5A; [54,117,118]) and its ablation could result in impaired RES recruitment. We compared the effect of *prp45*(1–169) on relative pre-mRNA levels with the effect of RES complex alleles *bud13Δ* and *ist3Δ*/*snu17Δ* [119,120], but we found no correlation. RES component Ist3/Snu17 is required for Mer1 dependent induction of *AMA1* and other Mer1-regulated meiotic genes [121]. Because *prp45*(1–169) cells undergo meiosis, the mutant must allow for the induction of *AMA1*, which implies that the recruitment of RES is achieved even in the absence of Prp45 chain (Figure 5A; [67]. We conclude that *prp45*(1–169) does not phenocopy RES complex alleles.

The Mediator complex is functionally linked to remodelling of chromatin in yeast promoters [95,96,122,123]. This can be illustrated by NGIs between alleles of Mediator components and complexes of SAGA, Paf1, and Ccr4-Not in the network of chromatin regulators constructed by Lenstra and co-workers (see Figure 4 in [23]). Two of the Mediator complex alleles, *srb2*Δ and *soh1*Δ, are included in the subnetwork enriched in *prp45*(1–169) NGIs (Figure 2C). The co-clustering of *srb2*Δ and *prp45*(1–169) may reflect the inefficient splicing of *SRB2*.

The vulnerability of splicing may be a useful thing to have

The outcome of the *prp45*(1–169) truncation can be summarized as an Htz1-sensitive failure to couple splicing to ongoing transcription. The interaction with *HTZ1* was bordering synthetic lethality and persisted even in the *srb2*Δi background. Less truncated variants of Prp45 maintained synthetic effect with *htz1*Δ on the level of pre-mRNA accumulation. We assume that the truncation of the 'rope' of Prp45 hampered the processes of snRNP recruitment during co-transcriptional spliceosome assembly [67]. For the same reason, the recycling of snRNPs may have been affected as well, breaking the 'supply chain' of splicing snRNPs. Intriguingly, lowering the demand for spliceosomes (see rapamycin experiment in SFig. S5A) partly rescued the splicing efficiency defect. The 'supply chain' problem could be related to deficient Prp22 recruitment [58], presumably because the truncation leaves Prp45(1–169) without the Prp22 interacting region (see Figures 1A and 5A). It was suggested that Prp22 and Prp16 depletion causes stalling of the first assembly steps via precursor depletion [124].

at 16°C or 30°C for the indicated number of days. (D) *prp45*(1–247) and *prp45*(1–330) mutants accumulated increased levels of pre-mRNA. The mRNA (left) and pre-mRNA levels (right) of *ECM33* and *ACT1* genes were measured by qPCR in WT, *prp45*(1–169), *prp45*(1–247), and *prp45*(1–330) cells. While the mRNA levels were approximately the same in all four strains, the pre-mRNAs were accumulated to the highest extent in *prp45*(1–169), followed by *prp45*(1–330). qPCR values were normalized to *TOM22* mRNA and expressed relative to WT strain. Error bars represent the standard deviation of four biological replicates for WT and *prp45*(1–169) cells and six biological replicates for *prp45*(1–247) and *prp45*(1–330) cells. (E) *prp45*(1–330) and *htz1*Δ negatively interacted on the level of pre-mRNA accumulation. The mRNA (left) and pre-mRNA levels (right) of *ECM33* and *COF1* genes were measured by qPCR in WT, *htz1*Δ, *prp45*(1–330) and *htz1*Δ *prp45*(1–330) cells. The pre-mRNAs showed highest accumulation in the double mutant. qPCR values were normalized to *TOM22* mRNA and expressed relative to WT strain. Error bars represent the standard deviation of 8 biological replicates. Statistical significance of the differences between strains in (D) and (E) is indicated as (*) for $p \le 0.05$, (**) for $p \le 0.01$, and (***) for $p \le 0.001$ based on the t-test with Holm correction for multiple testing (see methods and STab. 11).

In addition to delayed recruitment of trans-acting splicing factors, the truncation of Prp45 could affect the subsequent steps of mRNA maturation, including export. Because of the phenotype of its truncated versions, Prp45 could be regarded as a factor contributing to early steps of intron recognition. Defects in early acting splicing factors were found to be associated with intron retention [125]. It was assumed that the defective intron recognition [125,126] made the pre-mRNAs prone to escape because they would no longer interact properly with the surveillance and export systems [127–129]. As these latter systems also depend on nuclear structure [130] and chromatin state, including Htz1 metabolism [131], they also must be taken into account when considering the crosstalk between the splicing defect and *htz1* deletion [132]. In our screen, the alleles of the perinuclear quality control factors Mlp1 and Mlp2 [130] showed synthetic growth defects with *prp45*(1–169).

The *htz1*-sensitive phenotype of the *prp45*(1–169) mutant can be interpreted using any of the three models which describe the coupling between transcription and splicing in the literature (see Introduction). In the direct physical coupling scenario, Prp45 truncation could result in severing some of the specific physical contacts which are necessary to recruit the splicing apparatus to the emerging RNA. As part of an assembled spliceosome, the C terminal part of Prp45 is in contact with several Nineteen complex proteins, such as Cef1 and Syf2 (Figure 1A [133]). Nineteen complex is in turn implicated in connecting the transcription, splicing, and export complexes together with chromatin regulators [19,112,134,135]. The recruitment of the Nineteen complex, together with Prp45 itself, to some intron containing genes was assisted by the chromodomain protein Eaf3 [19]. In our screen, however, *eaf3* did not qualify as a hit. The physical connections between the complexes participating in gene expression may be redundant [13,136], some of them serving a particular type of promoter, chromosomal position of a gene or export pathway [137,138].

In the kinetic coupling scenario, the absence of splicing complexes from RNA PolII during delayed assembly in *prp45*(1–169) cells could affect RNA PolII parameters. Interference with splicing in budding yeast was found to affect RNA PolII distribution along intron containing genes, which led to the proposal of splicing-coupled transcription checkpoints [31,139]. Acting in the opposite direction, RNA PolII mutants were shown to modulate chromatin modifications along the body of genes and the degree of unidirectionality (the proportion of antisense transcription) at bidirectional promoters [44]. Slow PolII led to 3' to 5' shift of H3K36me modification, deposited by Set2, probably because PolII CTD Ser2 phosphorylation, responsible for Set2 recruitment, shifted as well [44].

In the indirect colocalization scenario, the concentration of properly matured snRNPs and splicing factors would not be sufficient for assembly because of defective or misplaced phase separation [140]. Both the lowered valency of the truncated Prp45 chain and *htz1* deletion could play contributing roles. Diffusion constants of nuclear RNPs are low, suggesting that the complexes engage in multiple transient interactions [141]. Liquid-liquid phase separation may result in their differential distribution, concentrating them to the vicinity of the processes for which they are needed. Misplaced (i.e. posttranscriptional) splicing may then face rate-limiting concentration of components needed for spliceosome assembly [142]. Notably, Prp45 has extensive regions of predicted intrinsic disorder [143]. It remains to be seen whether its conformational flexibility is only needed for spliceosome assembly [51,144], or whether it contributes to condensate formation [59,145]. The phase separation phenomena may also explain the disconnect between location and effect, which was repeatedly observed with regard to Htz1 [42,146–148].

Our data on Prp45 variants thus hint at two interesting aspects of splicing. First, the interactions of splicing factors preceding the moment of their final assembly (into spliceosome) decide on the speed of assembly and eventually determine the splicing efficiency. The problem of synergistic recruitment of proteins to RNA reflects the limits imposed by diffusion rates of snRNPs, and the speed and efficiency of recycling. A similar problem was addressed in the ribosome field, where the late associating ribosomal proteins were found to affect the early stages of ribosome assembly as chaperones through transient interactions with rRNA [149,150]. Second, Htz1 absence can aggravate the problem of hampered spliceosome assembly, suggesting the role of the chromatin environment in the splicing cycle. The cycle is prone to such vulnerability, as the spliceosome is assembled and disassembled for each cycle of catalysis and in many distinct locations. This vulnerability of splicing makes it a regulatory interface which the cells may use to modulate gene expression [11,142,151–153]. It should be interesting to learn more about the 'chaperoning phase' of splicing, which delivers the properly matured snRNPs to the sites of transcription at the right time. It is perhaps here that much of the chromatin-splicing interplay takes place.

Abbreviations

GO	gene ontology
NGI	negative genetic interaction
RPG	ribosomal protein gene
Subset_45	down regulated differentially scored transreads

Acknowledgments

We are grateful to the Boone Lab for the SGA data analyses. We thank members of the Sunnerhagen Lab for stimulating discussions. We thank Eva Krellerová for expert technical assistance and Dr. Marian Novotný for the molecular visualizations in Figure 1.

Disclosure statement

No potential conflict of interest was reported by the author(s).

Funding

The work of K.A. was funded by The Education for Competitiveness Operational Program (ECOP) and co-financed by the European Social Fund and the state budget of the Czech Republic (CZ.1.07/2.3.00/30.0022). We acknowledge the support of K.A. through the Marie Curie Host fellowship (QLK-CT2000-60036) and the EMBO Short Term Fellowship (ASTF 226-2005) during her stays in P. Sunnerhagen's Laboratory. The research was further supported by Charles University grants SVV260083, GAUK119710, GAUK441711, and GAUK8214, and the Swedish Cancer Fund (22-2014).

Data availability statement

The authors confirm that the data supporting the findings of this study are available within the article and its supplementary materials.

ORCID

Kateřina Abrhámová http://orcid.org/0000-0002-6299-8641
Ondřej Gahura http://orcid.org/0000-0002-2925-4763
František Půta http://orcid.org/0000-0002-8313-878X
Per Sunnerhagen http://orcid.org/0000-0002-0967-8729
Petr Folk http://orcid.org/0000-0003-3813-7777

References

[1] Herzel L, Ottoz DSM, Alpert T, et al. Splicing and transcription touch base: co-transcriptional spliceosome assembly and function. Nat Rev Mol Cell Biol. 2017;18(10):637–650. doi: 10.1038/nrm.2017.63
[2] Bentley DL. Coupling mRNA processing with transcription in time and space. Nat Rev Genet. 2014;15(3):163–175. doi: 10.1038/nrg3662
[3] Luco RF, Allo M, Schor IE, et al. Epigenetics in alternative pre-mRNA splicing. Cell. 2011;144(1):16–26. doi: 10.1016/j.cell.2010.11.056
[4] Costanzo M, VanderSluis B, Koch EN, et al. A global genetic interaction network maps a wiring diagram of cellular function. Science. 2016;353(6306):aaf1420–aaf 1420. doi: 10.1126/science.aaf1420
[5] Carrillo Oesterreich F, Preibisch S, Neugebauer KM. Global analysis of nascent RNA reveals transcriptional pausing in terminal exons. Mol Cell. 2010;40(4):571–581. doi: 10.1016/j.molcel.2010.11.004
[6] Carrillo Oesterreich F, Herzel L, Straube K, et al. Splicing of nascent RNA coincides with intron exit from RNA polymerase II. Cell. 2016;165(2):372–381. doi: 10.1016/j.cell.2016.02.045
[7] Khodor YL, Rodriguez J, Abruzzi KC, et al. Nascent-seq indicates widespread cotranscriptional pre-mRNA splicing in Drosophila. Genes Dev. 2011;25(23):2502–2512. doi: 10.1101/gad.178962.111
[8] Nojima T, Rebelo K, Gomes T, et al. RNA polymerase II phosphorylated on CTD serine 5 interacts with the spliceosome during Co-transcriptional Splicing. Mol Cell. 2018;72(2):369–379.e4. doi: 10.1016/j.molcel.2018.09.004
[9] Milligan L, Sayou C, Tuck A, et al. RNA polymerase II stalling at pre-mRNA splice sites is enforced by ubiquitination of the catalytic subunit. Elife. 2017;6:e27082. doi: 10.7554/eLife.27082
[10] Aslanzadeh V, Huang Y, Sanguinetti G, et al. Transcription rate strongly affects splicing fidelity and cotranscriptionality in budding yeast. Genome Res. 2018;28(2):203–213. doi: 10.1101/gr.225615.117
[11] Carrocci TJ, Neugebauer KM. Pre-mRNA splicing in the nuclear landscape. Cold Spring Harb Symp Quant Biol. 2019;84:11–20. doi: 10.1101/sqb.2019.84.040402
[12] Fica SM. Cryo-EM snapshots of the human spliceosome reveal structural adaptions for splicing regulation. Curr Opin Struct Biol. 2020;65:139–148. doi: 10.1016/j.sbi.2020.06.018
[13] Moehle EA, Ryan CJ, Krogan NJ, et al. The yeast SR-Like protein Npl3 links chromatin modification to mRNA processing. Buratowski S, editor. PLOS Genet. 2012;8(11):e1003101. doi: 10.1371/journal.pgen.1003101
[14] Minocha R, Popova V, Kopytova D, et al. Mud2 functions in transcription by recruiting the Prp19 and TREX complexes to transcribed genes. Nucleic Acids Res. 2018;46(18):9749–9763. doi: 10.1093/nar/gky640
[15] Cech TR. RNA in biological condensates. RNA. 2022;28(1):1–2. doi: 10.1261/rna.079051.121
[16] Gunderson FQ, Merkhofer EC, Johnson TL. Dynamic histone acetylation is critical for cotranscriptional spliceosome assembly and spliceosomal rearrangements. Proc Natl Acad Sci. 2011;108(5):2004–2009. doi: 10.1073/pnas.1011982108
[17] Hérissant L, Moehle EA, Bertaccini D, et al. H2B ubiquitylation modulates spliceosome assembly and function in budding yeast: histone marks and mRNA splicing. Biol Cell. 2014;106(4):126–138. doi: 10.1111/boc.201400003
[18] Sorenson MR, Jha DK, Ucles SA, et al. Histone H3K36 methylation regulates pre-mRNA splicing in Saccharomyces cerevisiae. RNA Biol. 2016;13(4):412–426. doi: 10.1080/15476286.2016.1144009
[19] Leung CS, Douglass SM, Morselli M, et al. H3K36 methylation and the chromodomain protein Eaf3 are required for proper cotranscriptional spliceosome assembly. Cell Rep. 2019;27(13):3760–3769.e4. doi: 10.1016/j.celrep.2019.05.100
[20] Shao W, Ding Z, Zheng Z-Z, et al. Prp5–Spt8/Spt3 interaction mediates a reciprocal coupling between splicing and transcription. Nucleic Acids Res. 2020;48(11):5799–5813. doi: 10.1093/nar/gkaa311
[21] Maudlin IE, Beggs JD. Spt5 modulates cotranscriptional spliceosome assembly in Saccharomyces cerevisiae. RNA. 2019;25(10):1298–1310. doi: 10.1261/rna.070425.119
[22] Martinkova K, Lebduska P, Skruzny M, et al. Functional mapping of Saccharomyces cerevisiae Prp45 identifies the SNW domain as essential for viability. J Biochem (Tokyo). 2002;132(4):557–563. doi: 10.1093/oxfordjournals.jbchem.a003257
[23] Lenstra TL, Benschop JJ, Kim T, et al. The specificity and topology of chromatin interaction pathways in yeast. Mol Cell. 2011;42(4):536–549. doi: 10.1016/j.molcel.2011.03.026
[24] Görnemann J, Kotovic KM, Hujer K, et al. Cotranscriptional spliceosome assembly occurs in a stepwise fashion and requires the cap binding complex. Mol Cell. 2005;19(1):53–63. doi: 10.1016/j.molcel.2005.05.007
[25] Haque N, Oberdoerffer S. Chromatin and splicing. Methods Mol Biol Clifton NJ. 2014;1126:97–113.
[26] Hnisz D, Shrinivas K, Young RA, et al. A phase separation model for transcriptional control. Cell. 2017;169(1):13–23. doi: 10.1016/j.cell.2017.02.007
[27] Henninger JE, Oksuz O, Shrinivas K, et al. RNA-Mediated feedback control of transcriptional condensates. Cell. 2021;184(1):207–225.e24. doi: 10.1016/j.cell.2020.11.030
[28] Bhat P, Honson D, Guttman M. Nuclear compartmentalization as a mechanism of quantitative control of gene expression. Nat Rev Mol Cell Biol. 2021;22(10):653–670. doi: 10.1038/s41580-021-00387-1
[29] Moehle EA, Braberg H, Krogan NJ, et al. Adventures in time and space: splicing efficiency and RNA polymerase II elongation rate. RNA Biol. 2014;11(4):313–319. doi: 10.4161/rna.28646
[30] Aslanzadeh V, Beggs JD. Revisiting the window of opportunity for cotranscriptional splicing in budding yeast. RNA. 2020;26(9):1081–1085. doi: 10.1261/rna.075895.120
[31] Chathoth KT, Barrass JD, Webb S, et al. A splicing-dependent transcriptional checkpoint associated with prespliceosome formation. Mol Cell. 2014;53(5):779–790. doi: 10.1016/j.molcel.2014.01.017
[32] Harlen KM, Trotta KL, Smith EE, et al. Comprehensive RNA polymerase II interactomes reveal distinct and varied roles for each phospho-CTD residue. Cell Rep. 2016;15(10):2147–2158. doi: 10.1016/j.celrep.2016.05.010
[33] Rosonina E, Yurko N, Li W, et al. Threonine-4 of the budding yeast RNAP II CTD couples transcription with Htz1-mediated chromatin remodeling. Proc Natl Acad Sci. 2014;111(33):11924–11931. doi: 10.1073/pnas.1412802111
[34] Lu H, Yu D, Hansen AS, et al. Phase-separation mechanism for C-terminal hyperphosphorylation of RNA polymerase II. Nature. 2018;558(7709):318–323. doi: 10.1038/s41586-018-0174-3
[35] Maita H, Nakagawa S. What is the switch for coupling transcription and splicing? RNA polymerase II C-terminal domain phosphorylation, phase separation and beyond. Wiley Interdiscip Rev RNA. 2020;11(1):e1574. doi: 10.1002/wrna.1574

[36] Guo YE, Manteiga JC, Henninger JE, et al. Pol II phosphorylation regulates a switch between transcriptional and splicing condensates. Nature. 2019;572(7770):543–548. doi: 10.1038/s41586-019-1464-0
[37] Church MC, Fleming AB. A role for histone acetylation in regulating transcription elongation. Transcription. 2018;9 (4):225–232. doi: 10.1080/21541264.2017.1394423
[38] Cohen E, Zafrir Z, Tuller T. A code for transcription elongation speed. RNA Biol. 2018;15(1):81–94. doi: 10.1080/15476286.2017.1384118
[39] Rahhal R, Seto E. Emerging roles of histone modifications and HDACs in RNA splicing. Nucleic Acids Res. 2019;47 (10):4911–4926. doi: 10.1093/nar/gkz292
[40] Guillemette B, Gaudreau L. Reuniting the contrasting functions of H2A.Z. This paper is one of a selection of papers published in this special issue, entitled 27th international west coast chromatin and chromosome conference, and has undergone the Journal's usual peer review process. Biochem Cell Biol Biochim Biol Cell. 2006;84 (4):528–535. doi: 10.1139/o06-077
[41] Billon P, Côté J. Precise deposition of histone H2A.Z in chromatin for genome expression and maintenance. Biochim Biophys Acta Gene Regul Mech. 2012;1819(3–4):290–302. doi: 10.1016/j.bbagrm.2011.10.004
[42] Brewis HT, Wang AY, Gaub A, et al. What makes a histone variant a variant: changing H2A to become H2A.Z. Schneider R, editor. PLOS Genet. 2021;17(12):e1009950. doi: 10.1371/journal.pgen.1009950
[43] Sims RJ, Millhouse S, Chen C-F, et al. Recognition of trimethylated histone H3 lysine 4 facilitates the recruitment of transcription postinitiation factors and pre-mRNA splicing. Mol Cell. 2007;28(4):665–676. doi: 10.1016/j.molcel.2007.11.010
[44] Fong N, Saldi T, Sheridan RM, et al. RNA Pol II dynamics modulate co-transcriptional chromatin modification, CTD phosphorylation, and transcriptional direction. Mol Cell. 2017;66(4):546–557.e3. doi: 10.1016/j.molcel.2017.04.016
[45] Patrick KL, Ryan CJ, Xu J, et al. Genetic interaction mapping reveals a role for the SWI/SNF nucleosome remodeler in spliceosome activation in fission yeast. Bentley D, editor. PLOS Genet. 2015;11(3):e1005074. doi: 10.1371/journal.pgen.1005074
[46] Nissen KE, Homer CM, Ryan CJ, et al. The histone variant H2A.Z promotes splicing of weak introns. Genes Dev. 2017;31 (7):688–701. doi: 10.1101/gad.295287.116
[47] Neves LT, Douglass S, Spreafico R, et al. The histone variant H2A.Z promotes efficient cotranscriptional splicing in *S. cerevisiae*. Genes Dev. 2017;31(7):702–717. doi: 10.1101/gad.295188.116
[48] Bai R, Yan C, Wan R, et al. Structure of the post-catalytic spliceosome from Saccharomyces cerevisiae. Cell. 2017;171(7):1589–1598.e8. doi: 10.1016/j.cell.2017.10.038
[49] Jumper J, Evans R, Pritzel A, et al. Highly accurate protein structure prediction with AlphaFold. Nature. 2021;596 (7873):583–589. doi: 10.1038/s41586-021-03819-2
[50] Ruff KM, Pappu RV. AlphaFold and implications for intrinsically disordered proteins. J Mol Biol. 2021;433(20):167208. doi: 10.1016/j.jmb.2021.167208
[51] Wan R, Bai R, Yan C, et al. Structures of the catalytically activated yeast spliceosome reveal the mechanism of branching. Cell. 2019;177(2):339–351.e13. doi: 10.1016/j.cell.2019.02.006
[52] Albers M, Diment A, Muraru M. Identification and characterization of Prp45p and Prp46p, essential pre-mRNA splicing factors. RNA. 2003;9(1):138–150. doi: 10.1261/rna.2119903
[53] Wan R, Bai R, Zhan X, et al. How is precursor messenger RNA spliced by the spliceosome? Annu Rev Biochem. 2020;89 (1):333–358. doi: 10.1146/annurev-biochem-013118-111024
[54] Yan C, Wan R, Bai R, et al. Structure of a yeast step II catalytically activated spliceosome. Science. 2017;355(6321):149–155. doi: 10.1126/science.aak9979
[55] Plaschka C, Newman AJ, Nagai K. Structural basis of nuclear pre-mRNA splicing: lessons from yeast. Cold Spring Harb Perspect Biol. 2019;11(5):a032391. doi: 10.1101/cshperspect.a032391
[56] Wilkinson ME, Fica SM, Galej WP, et al. Postcatalytic spliceosome structure reveals mechanism of 3′–splice site selection. Science. 2017;358(6368):1283–1288. doi: 10.1126/science.aar3729
[57] Wan R, Yan C, Bai R, et al. Structure of an intron lariat spliceosome from *Saccharomyces cerevisiae*. Cell. 2017;171(1):120–132. e12. doi: 10.1016/j.cell.2017.08.029
[58] Gahura O, Abrhámová K, Skružný M, et al. Prp45 affects Prp22 partition in spliceosomal complexes and splicing efficiency of non-consensus substrates. J Cell Biochem. 2009;106(1):139–151. doi: 10.1002/jcb.21989
[59] Harmon TS, Holehouse AS, Rosen MK, et al. Intrinsically disordered linkers determine the interplay between phase separation and gelation in multivalent proteins. Elife. 2017;6:e30294. doi: 10.7554/eLife.30294
[60] Zhang C, Baudino TA, Dowd DR, et al. Ternary complexes and cooperative interplay between NCoA-62/Ski-interacting protein and steroid receptor coactivators in vitamin D receptor-mediated transcription. J Biol Chem. 2001;276 (44):40614–40620. doi: 10.1074/jbc.M106263200
[61] Prathapam T, Kühne C, Banks L. Skip interacts with the retinoblastoma tumor suppressor and inhibits its transcriptional repression activity. Nucleic Acids Res. 2002;30(23):5261–5268. doi: 10.1093/nar/gkf658
[62] Brès V, Gomes N, Pickle L, et al. A human splicing factor, SKIP, associates with P-TEFb and enhances transcription elongation by HIV-1 Tat. Genes Dev. 2005;19(10):1211–1226. doi: 10.1101/gad.1291705
[63] Chen Y, Zhang L, Jones KA. SKIP counteracts p53-mediated apoptosis via selective regulation of $p21^{Cip1}$ mRNA splicing. Genes Dev. 2011;25(7):701–716. doi: 10.1101/gad.2002611
[64] Brès V, Yoh SM, Jones KA. The multi-tasking P-TEFb complex. Curr Opin Cell Biol. 2008;20(3):334–340. doi: 10.1016/j.ceb.2008.04.008
[65] Újvári A, Luse DS. Newly initiated RNA encounters a factor involved in splicing immediately upon emerging from within RNA polymerase II. J Biol Chem. 2004;279(48):49773–49779. doi: 10.1074/jbc.M409087200
[66] Ambrozková M, Půta F, Fuková I, et al. The fission yeast ortholog of the coregulator SKIP interacts with the small subunit of U2AF. Biochem Biophys Res Commun. 2001;284(5):1148–1154. doi: 10.1006/bbrc.2001.5108
[67] Hálová M, Gahura O, Převorovský M, et al. Nineteen complex–related factor Prp45 is required for the early stages of cotranscriptional spliceosome assembly. RNA. 2017;23(10):1512–1524. doi: 10.1261/rna.061986.117
[68] Clark TA, Sugnet CW, Ares M. Genomewide analysis of mRNA processing in yeast using splicing-specific microarrays. Science. 2002;296(5569):907–910. doi: 10.1126/science.1069415
[69] Soutourina J. Transcription regulation by the mediator complex. Nat Rev Mol Cell Biol. 2018;19(4):262–274. doi: 10.1038/nrm.2017.115
[70] Van Driessche B, Tafforeau L, Hentges P, et al. Additional vectors for PCR-based gene tagging in *Saccharomyces cerevisiae and Schizosaccharomyces pombe* using nourseothricin resistance. Yeast Chichester Engl. 2005;22(13):1061–1068. doi: 10.1002/yea.1293
[71] Storici F, Lewis LK, Resnick MA. In vivo site-directed mutagenesis using oligonucleotides. Nat Biotechnol. 2001;19(8):773–776. doi: 10.1038/90837
[72] Tong AHY, Boone C. Synthetic genetic array analysis in *Saccharomyces cerevisiae*. Methods Mol Biol Clifton NJ. 2006;313:171–192.
[73] Winzeler EA, Shoemaker DD, Astromoff A, et al. Functional characterization of the *S. cerevisiae* genome by gene deletion and parallel analysis. Science. 1999;285(5429):901–906. doi: 10.1126/science.285.5429.901
[74] Livak KJ, Schmittgen TD. Analysis of relative gene expression data using real-time quantitative PCR and the 2−ΔΔCT method. Methods. 2001;25(4):402–408. doi: 10.1006/meth.2001.1262

[75] Převorovský M, Hálová M, Abrhámová K, et al. Workflow for genome-wide determination of pre-mRNA splicing efficiency from yeast RNA-seq data. Biomed Res Int. 2016;2016:1–9. doi: 10.1155/2016/4783841
[76] Baryshnikova A. Systematic functional annotation and visualization of biological networks. Cell Syst. 2016;2(6):412–421. doi: 10.1016/j.cels.2016.04.014
[77] Persson BL, Lagerstedt JO, Pratt JR, et al. Regulation of phosphate acquisition in *Saccharomyces cerevisiae*. Curr Genet. 2003;43(4):225–244. doi: 10.1007/s00294-003-0400-9
[78] Carvin CD, Kladde MP. Effectors of Lysine 4 methylation of histone H3 in *Saccharomyces cerevisiae* are negative regulators of PHO5 and GAL1-10. J Biol Chem. 2004;279(32):33057–33062. doi: 10.1074/jbc.M405033200
[79] Ellison MA, Lederer AR, Warner MH, et al. The Paf1 complex broadly impacts the transcriptome of *Saccharomyces cerevisiae*. Genetics. 2019;212(3):711–728. doi: 10.1534/genetics.119.302262
[80] Query CC, Konarska MM. Suppression of multiple substrate mutations by spliceosomal prp8 alleles suggests functional correlations with ribosomal ambiguity mutants. Mol Cell. 2004;14(3):343–354. doi: 10.1016/S1097-2765(04)00217-5
[81] Konarska MM, Vilardell J, Query CC. Repositioning of the reaction intermediate within the catalytic center of the spliceosome. Mol Cell. 2006;21(4):543–553. doi: 10.1016/j.molcel.2006.01.017
[82] Chung NC, Miasojedow B, Startek M, et al. Jaccard/Tanimoto similarity test and estimation methods for biological presence-absence data. BMC Bioinf. 2019;20(S15):644. doi: 10.1186/s12859-019-3118-5
[83] Gu M, Naiyachit Y, Wood TJ, et al. H2A.Z marks antisense promoters and has positive effects on antisense transcript levels in budding yeast. BMC Genomics. 2015;16(1):99. doi: 10.1186/s12864-015-1247-4
[84] Sorenson MR, Stevens SW. Rapid identification of mRNA processing defects with a novel single-cell yeast reporter. RNA. 2014;20(5):732–745. doi: 10.1261/rna.042663.113
[85] Sun M, Schwalb B, Pirkl N, et al. Global analysis of eukaryotic mRNA degradation reveals Xrn1-dependent buffering of transcript levels. Mol Cell. 2013;52(1):52–62. doi: 10.1016/j.molcel.2013.09.010
[86] Pettersen EF, Goddard TD, Huang CC, et al. UCSF ChimeraX: structure visualization for researchers, educators, and developers. Protein Sci Publ Protein Soc. 2021;30(1):70–82. doi: 10.1002/pro.3943
[87] Dion MF, Kaplan T, Kim M, et al. Dynamics of replication-independent histone turnover in budding yeast. Science. 2007;315(5817):1405–1408. doi: 10.1126/science.1134053
[88] Abrhámová K, Nemčko F, Libus J, et al. Introns provide a platform for intergenic regulatory feedback of RPL22 paralogs in yeast. Palazzo AF, editor. PLOS ONE. 2018;13(1):e0190685. doi: 10.1371/journal.pone.0190685
[89] Herzel L, Neugebauer KM. Quantification of co-transcriptional splicing from RNA-Seq data. Methods. 2015;85:36–43. doi: 10.1016/j.ymeth.2015.04.024
[90] VanderSluis B, Costanzo M, Billmann M, et al. Integrating genetic and protein–protein interaction networks maps a functional wiring diagram of a cell. Curr Opin Microbiol. 2018;45:170–179. doi: 10.1016/j.mib.2018.06.004
[91] Yang X, Shen Y, Garre E, et al. Stress granule-defective mutants deregulate stress responsive transcripts. Anderson P, editor. PLOS Genet. 2014;10(11):e1004763. doi: 10.1371/journal.pgen.1004763
[92] Tavella TA, Cassiano GC, Costa FTM, et al. Yeast-based high-throughput screens for discovery of kinase inhibitors for neglected diseases. Adv Protein Chem Struct Biol. 2021;124:275–309.
[93] Shannon P, Markiel A, Ozier O, et al. Cytoscape: a software environment for integrated models of biomolecular interaction networks. Genome Res. 2003;13(11):2498–2504. doi: 10.1101/gr.1239303
[94] Kuras L, Borggrefe T, Kornberg RD. Association of the mediator complex with enhancers of active genes. Proc Natl Acad Sci. 2003;100(24):13887–13891. doi: 10.1073/pnas.2036346100
[95] Larschan E, Winston F. The Saccharomyces cerevisiae Srb8-Srb11 complex functions with the SAGA complex during Gal4-activated transcription. Mol Cell Biol. 2005;25(1):114–123. doi: 10.1128/MCB.25.1.114-123.2005
[96] Nagai S, Davis RE, Mattei PJ, et al. Chromatin potentiates transcription. Proc Natl Acad Sci. 2017;114(7):1536–1541. doi: 10.1073/pnas.1620312114
[97] Munding EM, Shiue L, Katzman S, et al. Competition between pre-mRNAs for the splicing machinery drives global regulation of splicing. Mol Cell. 2013;51(3):338–348. doi: 10.1016/j.molcel.2013.06.012
[98] Shore D, Zencir S, Albert B. Transcriptional control of ribosome biogenesis in yeast: links to growth and stress signals. Biochem Soc Trans. 2021;49(4):1589–1599. doi: 10.1042/BST20201136
[99] Wilkinson ME, Charenton C, Nagai K. RNA splicing by the spliceosome. Annu Rev Biochem. 2020;89(1):359–388. doi: 10.1146/annurev-biochem-091719-064225
[100] Bagchi DN, Battenhouse AM, Park D, et al. The histone variant H2A.Z in yeast is almost exclusively incorporated into the +1 nucleosome in the direction of transcription. Nucleic Acids Res. 2019:gkz1075. doi: 10.1093/nar/gkz1075
[101] Iyer VR. The specificity of H2A.Z occupancy in the yeast genome and its relationship to transcription. Curr Genet. 2020;66(5):939–944. doi: 10.1007/s00294-020-01087-7
[102] Holstege FCP, Jennings EG, Wyrick JJ, et al. Dissecting the regulatory circuitry of a eukaryotic genome. Cell. 1998;95(5):717–728. doi: 10.1016/S0092-8674(00)81641-4
[103] Basehoar AD, Zanton SJ, Pugh BF. Identification and distinct regulation of yeast TATA box-containing genes. Cell. 2004;116(5):699–709. doi: 10.1016/S0092-8674(04)00205-3
[104] Van Oss SB, Cucinotta CE, Arndt KM. Emerging insights into the roles of the Paf1 complex in gene regulation. Trends Biochem Sci. 2017;42(10):788–798. doi: 10.1016/j.tibs.2017.08.003
[105] Fischl H, Howe FS, Furger A, et al. Paf1 has distinct roles in transcription elongation and differential transcript fate. Mol Cell. 2017;65(4):685–698.e8. doi: 10.1016/j.molcel.2017.01.006
[106] Song Y-H, Ahn SH. A Bre1-associated protein, large 1 (Lge1), promotes H2B ubiquitylation during the early stages of transcription elongation. J Biol Chem. 2010;285(4):2361–2367. doi: 10.1074/jbc.M109.039255
[107] Venkatasubrahmanyam S, Hwang WW, Meneghini MD, et al. Genome-wide, as opposed to local, antisilencing is mediated redundantly by the euchromatic factors Set1 and H2A. Proc Natl Acad Sci, USA. 2007;104(42):16609–16614. doi: 10.1073/pnas.0700914104
[108] Sayou C, Millán-Zambrano G, Santos-Rosa H, et al. RNA binding by histone methyltransferases Set1 and Set2. Mol Cell Biol. 2017;37(14):e00165–17. doi: 10.1128/MCB.00165-17
[109] Hang M, Smith MM. Genetic analysis implicates the Set3/Hos2 histone deacetylase in the deposition and remodeling of nucleosomes containing H2A.Z. Genetics. 2011;187(4):1053–1066. doi: 10.1534/genetics.110.125419
[110] Krogan NJ, Kim M, Tong A, et al. Methylation of histone H3 by Set2 in Saccharomyces cerevisiae is linked to transcriptional elongation by RNA polymerase II. Mol Cell Biol. 2003;23(12):4207–4218. doi: 10.1128/MCB.23.12.4207-4218.2003
[111] Jaiswal D, Turniansky R, Green EM. Choose your own adventure: the role of histone modifications in yeast cell fate. J Mol Biol. 2017;429(13):1946–1957. doi: 10.1016/j.jmb.2016.10.018
[112] Larson A, Fair BJ, Pleiss JA. Interconnections between RNA-processing pathways revealed by a sequencing-based genetic screen for pre-mRNA splicing mutants in fission yeast. G3: Genes | Genomes | Genetics. 2016;6(6):1513–1523. doi: 10.1534/g3.116.027508
[113] Hwang WW, Venkatasubrahmanyam S, Ianculescu AG, et al. A conserved RING finger protein required for histone H2B monoubiquitination and cell size control. Mol Cell. 2003;11(1):261–266. doi: 10.1016/S1097-2765(02)00826-2
[114] Pleiss JA, Whitworth GB, Bergkessel M, et al. Transcript specificity in yeast pre-mRNA splicing revealed by mutations in core

spliceosomal components. Black DL, editor. PLOS Biol. 2007;5(4):e90. doi: 10.1371/journal.pbio.0050090
[115] Brown T, Howe FS, Murray SC, et al. Antisense transcription-dependent chromatin signature modulates sense transcript dynamics. Mol Syst Biol. 2018;14(2):e8007. doi: 10.15252/msb.20178007
[116] Zhou Y, Johansson MJO. The pre-mRNA retention and splicing complex controls expression of the mediator subunit Med20. RNA Biol. 2017;14(10):1411–1417. doi: 10.1080/15476286.2017.1294310
[117] Bao P, Will CL, Urlaub H, et al. The RES complex is required for efficient transformation of the precatalytic B spliceosome into an activated B^{act} complex. Genes Dev. 2017;31(23–24):2416–2429. doi: 10.1101/gad.308163.117
[118] Rauhut R, Fabrizio P, Dybkov O, et al. Molecular architecture of the Saccharomyces cerevisiae activated spliceosome. Science. 2016;353(6306):1399–1405. doi: 10.1126/science.aag1906
[119] Zhou Y, Chen C, Johansson MJO. The pre-mRNA retention and splicing complex controls tRNA maturation by promoting TAN1 expression. Nucleic Acids Res. 2013;41(11):5669–5678. doi: 10.1093/nar/gkt269
[120] Scherrer FW, Spingola M. A subset of Mer1p-dependent introns requires Bud13p for splicing activation and nuclear retention. RNA. 2006;12(7):1361–1372. doi: 10.1261/rna.2276806
[121] Spingola M. Mer1p is a modular splicing factor whose function depends on the conserved U2 snRNP protein Snu17p. Nucleic Acids Res. 2004;32(3):1242–1250. doi: 10.1093/nar/gkh281
[122] He Q, Battistella L, Morse RH. Mediator requirement downstream of chromatin remodeling during transcriptional activation of CHA1 in yeast. J Biol Chem. 2008;283(9):5276–5286. doi: 10.1074/jbc.M708266200
[123] Cho W-K, Spille J-H, Hecht M, et al. Mediator and RNA polymerase II clusters associate in transcription-dependent condensates. Science. 2018;361(6400):412–415. doi: 10.1126/science.aar4199
[124] Mendoza-Ochoa GI, Barrass JD, Maudlin IE, et al. Blocking late stages of splicing quickly limits pre-spliceosome assembly in vivo. RNA Biol. 2019;16(12):1775–1784. doi: 10.1080/15476286.2019.1657788
[125] Rutz B. A dual role for BBP/ScSF1 in nuclear pre-mRNA retention and splicing. Embo J. 2000;19(8):1873–1886. doi: 10.1093/emboj/19.8.1873
[126] Legrain P, Rosbash M. Some cis- and trans-acting mutants for splicing target pre-mRNA to the cytoplasm. Cell. 1989;57(4):573–583. doi: 10.1016/0092-8674(89)90127-X
[127] Baejen C, Torkler P, Gressel S, et al. Transcriptome maps of mRNP biogenesis factors define pre-mRNA recognition. Mol Cell. 2014;55(5):745–757. doi: 10.1016/j.molcel.2014.08.005
[128] Björk P, Wieslander L. Integration of mRNP formation and export. Cell Mol Life Sci. 2017;74(16):2875–2897. doi: 10.1007/s00018-017-2503-3
[129] Wang K, Yin C, Du X, et al. A U2-snRNP–independent role of SF3b in promoting mRNA export. Proc Natl Acad Sci. 2019;116(16):7837–7846. doi: 10.1073/pnas.1818835116
[130] Galy V, Gadal O, Fromont-Racine M, et al. Nuclear retention of unspliced mRNAs in yeast is mediated by perinuclear Mlp1. Cell. 2004;116(1):63–73. doi: 10.1016/S0092-8674(03)01026-2
[131] Gardner JM, Smoyer CJ, Stensrud ES, et al. Targeting of the SUN protein Mps3 to the inner nuclear membrane by the histone variant H2A.Z. J Cell Bio. 2011;193(3):489–507. doi: 10.1083/jcb.201011017
[132] Bonde MM, Voegeli S, Baudrimont A, et al. Quantification of pre-mRNA escape rate and synergy in splicing. Nucleic Acids Res. 2014;42(20):12847–12860. doi: 10.1093/nar/gku1014
[133] de Moura TR, Mozaffari-Jovin S, Szabó CZK, et al. Prp19/Pso4 is an autoinhibited ubiquitin ligase activated by stepwise assembly of three splicing factors. Mol Cell. 2018;69(6):979–992.e6. doi: 10.1016/j.molcel.2018.02.022
[134] Chanarat S, Sträßer K. Splicing and beyond: the many faces of the Prp19 complex. Biochim Biophys Acta BBA – Mol Cell Res. 2013;1833:2126–2134. doi: 10.1016/j.bbamcr.2013.05.023
[135] Chanarat S, Seizl M, Sträßer K. The Prp19 complex is a novel transcription elongation factor required for TREX occupancy at transcribed genes. Genes Dev. 2011;25(11):1147–1158. doi: 10.1101/gad.623411
[136] Kress TL, Krogan NJ, Guthrie C. A single SR-like protein, Npl3, promotes pre-mRNA splicing in budding yeast. Mol Cell. 2008;32(5):727–734. doi: 10.1016/j.molcel.2008.11.013
[137] Sayani S, Chanfreau GF. Sequential RNA degradation pathways provide a fail-safe mechanism to limit the accumulation of unspliced transcripts in Saccharomyces cerevisiae. RNA. 2012;18(8):1563–1572. doi: 10.1261/rna.033779.112
[138] Xie Y, Ren Y. Mechanisms of nuclear mRNA export: a structural perspective. Traffic. 2019;20(11):829–840. doi: 10.1111/tra.12691
[139] Alexander RD, Innocente SA, Barrass JD, et al. Splicing-dependent RNA polymerase pausing in yeast. Mol Cell. 2010;40(4):582–593. doi: 10.1016/j.molcel.2010.11.005
[140] Chen H, Pugh BF. What do transcription factors interact with? J Mol Biol. 2021;433(14):166883. doi: 10.1016/j.jmb.2021.166883
[141] Huranová M, Ivani I, Benda A, et al. The differential interaction of snRnps with pre-mRNA reveals splicing kinetics in living cells. J Cell Bio. 2010;191(1):75–86. doi: 10.1083/jcb.201004030
[142] Neugebauer KM. Nascent RNA and the coordination of splicing with transcription. Cold Spring Harb Perspect Biol. 2019;11(8):a032227. doi: 10.1101/cshperspect.a032227
[143] de Coelho Ribeiro ML, Espinosa J, Islam S, et al. Malleable ribonucleoprotein machine: protein intrinsic disorder in the *Saccharomyces cerevisiae spliceosome*. PeerJ. 2013;1:e2. doi: 10.7717/peerj.2
[144] van der Feltz C, Hoskins AA. Structural and functional modularity of the U2 snRNP in pre-mRNA splicing. Crit Rev Biochem Mol Biol. 2019;54(5):443–465. doi: 10.1080/10409238.2019.1691497
[145] Harlen KM, Churchman LS. The code and beyond: transcription regulation by the RNA polymerase II carboxy-terminal domain. Nat Rev Mol Cell Biol. 2017;18(4):263–273. doi: 10.1038/nrm.2017.10
[146] Lin Y, Protter DSW, Rosen MK, et al. Formation and maturation of phase-separated liquid droplets by RNA-Binding proteins. Mol Cell. 2015;60(2):208–219. doi: 10.1016/j.molcel.2015.08.018
[147] Guo Q, Shi X, Wang X. RNA and liquid-liquid phase separation. Non-Coding RNA Res. 2021;6(2):92–99. doi: 10.1016/j.ncrna.2021.04.003
[148] Shaban HA, Barth R, Bystricky K. Navigating the crowd: visualizing coordination between genome dynamics, structure, and transcription. Genome Biol. 2020;21(1):278. doi: 10.1186/s13059-020-02185-y
[149] Duss O, Stepanyuk GA, Puglisi JD, et al. Transient protein-RNA interactions guide nascent ribosomal RNA folding. Cell. 2019;179(6):1357–1369.e16. doi: 10.1016/j.cell.2019.10.035
[150] Rodgers ML, Woodson SA. Transcription increases the cooperativity of ribonucleoprotein assembly. Cell. 2019;179(6):1370–1381.e12. doi: 10.1016/j.cell.2019.11.007
[151] Frumkin I, Yofe I, Bar-Ziv R, et al. Evolution of intron splicing towards optimized gene expression is based on various cis- and trans-molecular mechanisms. Hurst LD, editor. PLOS Biol. 2019;17(8):e3000423. doi: 10.1371/journal.pbio.3000423
[152] Liao SE, Regev O. Splicing at the phase-separated nuclear speckle interface: a model. Nucleic Acids Res. 2021;49(2):636–645. doi: 10.1093/nar/gkaa1209
[153] Gordon JM, Phizicky DV, Neugebauer KM. Nuclear mechanisms of gene expression control: pre-mRNA splicing as a life or death decision. Curr Opin Genet Dev. 2021;67:67–76. doi: 10.1016/j.gde.2020.11.002